OXFORD

ORIGINAL ARTICLE

# Pharmacological Modulation of AMPAR Rescues Intellectual Disability-Like Phenotype in *Tm4sf2*[−/y] Mice

Luca Murru[1], Elena Vezzoli[2,3,7], Anna Longatti[1,3], Luisa Ponzoni[2,4], Andrea Falqui[5], Alessandra Folci[1], Edoardo Moretto[1], Veronica Bianchi[6], Daniela Braida[2], Mariaelvina Sala[1], Patrizia D'Adamo[6], Silvia Bassani[1], Maura Francolini[2] and Maria Passafaro[1]

[1]CNR Institute of Neuroscience, 20129 Milano, Italy, [2]Department of Medical Biotechnology and Translational Medicine, Università degli studi di Milano, Via Vanvitelli 32, 20129 Milano, Italy, [3]Department of Pharmacological and Biomolecular Sciences (DiSFeB), Università di Milano, Via Balzaretti 9, 20133 Milano, Italy, [4]Fondazione Umberto Veronesi, Piazza Velasca 5, 20122 Milan, Italy, [5]Biological and Environmental Sciences and Engineering Division, King Abdullah University for Science and Technology (KAUST), Thuwal 23955-6900, Kingdom of Saudi Arabia, [6]Division of Neuroscience, IRCSS San Raffaele Scientific Institute, 20132 Milan, Italy and [7]Present address: Department of Biosciences and Centre for Stem Cell Research, University of Milan and Istituto Nazionale di Genetica Molecolare "Romeo ed Enrica Invernizzi" Milan, Italy

Address correspondence to Maria Passafaro, Via L. Vanvitelli 32, 20129 Milan, Italy. Email: m.passafaro@in.cnr.it

## Abstract

Intellectual disability affects 2–3% of the world's population and typically begins during childhood, causing impairments in social skills and cognitive abilities. Mutations in the *TM4SF2* gene, which encodes the TSPAN7 protein, cause a severe form of intellectual disability, and currently, no therapy is able to ameliorate this cognitive impairment. We previously reported that, in cultured neurons, shRNA-mediated down-regulation of TSPAN7 affects AMPAR trafficking by enhancing PICK1–GluA2 interaction, thereby increasing the intracellular retention of AMPAR. Here, we found that loss of TSPAN7 function in mice causes alterations in hippocampal excitatory synapse structure and functionality as well as cognitive impairment. These changes occurred along with alterations in AMPAR expression levels. We also found that interfering with PICK1–GluA2 binding restored synaptic function in *Tm4sf2*[−/y] mice. Moreover, potentiation of AMPAR activity via the administration of the ampakine CX516 reverted the neurological phenotype observed in *Tm4sf2*[−/y] mice, suggesting that pharmacological modulation of AMPAR may represent a new approach for treating patients affected by *TM4SF2* mutations and intellectual disability.

**Key words:** ampakine, animal model, hippocampus, ID, TSPAN7

## Introduction

The tetraspanin family of proteins is widely expressed and conserved in eukaryotic cells, with 33 different tetraspanins being expressed in human tissues (Tarrant et al. 2003; Charrin et al. 2009, 2014; Jiang et al. 2015). Structurally, these proteins are characterized by 4 transmembrane domains, 2 extracellular loops and short intracellular N- and C- termini (Hemler 2005).

A main feature of tetraspanins is their ability to interact with other proteins such as integrins, membrane receptors and signaling molecules (Bassani and Cingolani 2012; Bassani and Passafaro 2012). Such interactions lead to the formation of tetraspanin-enriched microdomains (TEMs) on the cell surface, which regulate transmembrane protein signaling, trafficking, and biosynthetic processing (Maecker et al. 1997; Hemler 1998, 2008; Yauch and Hemler 2000; Chavis and Westbrook 2001).

Tetraspanins play roles in many biological processes, including immune system functioning (Jones et al. 2011; van Spriel 2011; Levy 2014), cancer progression or metastasis formation (Boucheix and Rubinstein 2001; Zoller 2009; Romanska and Berditchevski 2011; Hemler 2014), and intercellular communication via extracellular vesicles (Andreu and Yanez-Mo 2014).

The *TM4SF2* gene encodes the tetraspanin7 (TSPAN7) protein, which is highly expressed in the central nervous system (CNS), particularly in the frontal cortex, olfactory bulb, cerebellum and hippocampus (Zemni et al. 2000). Importantly, nonsyndromic X-linked intellectual disability (XLID) (Piton et al. 2011; Bassani et al. 2013; Penzes et al. 2013) has been associated with mutations in this gene, including X;2 balanced translocation, a nonsense mutation that results in a premature stop codon TGA (gly218-to-ter), a point mutation (P172H) substituting a single amino acid (Zemni et al. 2000), and a 2-bp deletion (564delGT) that results in a premature stop codon at position 192 (Abidi et al. 2002). Both the gly218-to-ter nonsense mutation and the 2-bp deletion are predicted to produce a truncated protein lacking the fourth transmembrane domain and the cytoplasmic C-terminal tail.

We previously found that TSPAN7 promotes the formation of filopodia and dendritic spines and is required for spine stability and normal synaptic transmission in cultured hippocampal neurons. Furthermore, we identified protein interacting with C kinase 1 (PICK1) as a binding partner of TSPAN7 (Bassani et al. 2012). PICK1 is involved in the internalization and recycling of AMPA receptor (AMPAR) (Perez et al. 2001), and TSPAN7 appears to regulate the association between PICK1 and AMPAR, thereby controlling AMPAR trafficking and internalization (Bassani et al. 2012). Additionally, TSPAN7 has been shown to promote $D_2$ dopamine receptor internalization (Lee et al. 2017).

In the present study, we showed that absence of TSPAN7 in the brains of $Tm4sf2^{-/y}$ mice caused alterations in excitatory postsynapse structure, function and plasticity as well as impairment in hippocampal-related learning and memory behavior. In addition, $Tm4sf2^{-/y}$ mice showed an increased AMPA rectification index (RI) compared with $Tm4sf2^{+/y}$ mice, indicating that less GluA2-containing AMPAR was present at the cell surface. Interestingly, interference on PICK1–GluA2 binding or treatment with CX516, a positive modulator of AMPAR, rescued the ID phenotype. These findings suggest that modulation of AMPAR could represent a new therapeutic strategy for ID caused by *TM4SF2* mutations.

## Materials and Methods

### Animals

$Tm4sf2^{+/y}$ and $Tm4sf2^{-/y}$ 30–90 days old male mice were housed in polycarbonate cages with food and water ad libitum. Cob-bedding was changed weekly, and the animal house was 21 °C with a 12 h light cycle (lights on at 08:00) if not stated otherwise. All the experiments followed the guidelines established by the Italian Council on Animal Care and were approved by the Italian Government decree No. 747/2015-PR, if not stated otherwise. All efforts were made to minimize the number of subjects used and their suffering. The 3 mice per genotype/age/treatment were used for electron microscopy (EM), 3–9 mice per genotype at 90 days for biochemical and crosslinking assays. For electrophysiology and behavioral analysis 3 mice 60 days old per genotype/treatment and at least 7 mice 90 days old per genotype/treatment were used, respectively.

### Histological Analyses

Mice were anesthetized by intraperitoneal injection of 10 mg/ml avertine (Sigma) and transcardially perfused with 4% paraformaldehyde in 0.1 M phosphate buffer (pH 7.4). Dissected brains were further fixed for 48 h at 4 °C before paraffin embedding and sectioning. Four micrometers sections were stained with hematoxylin and eosin and examined under the optical microscope.

### Electron microscopy

Sample preparation for transmission electron microscopy (TEM) and quantitative analyses on TEM images were performed as described (Folci et al. 2016). Briefly, mice were anesthetized by intraperitoneal injection of 10 mg/ml avertine (Sigma) and transcardially perfused with 2.5% glutaraldehyde, 2% paraformaldehyde in 0.15 M sodium cacodylate buffer (pH 7.4). Dissected brains were postfixed for additional 24 h at 4 °C. Coronal sections (100 μm thickness) where obtained with a vibratome (Leica VT1000S, Leica Microsystems, Austria) and selected brain areas were manually dissected. After washing, samples were postfixed with 2% osmium tetroxide, rinsed, en bloc stained with 1% uranyl acetate in water for 45 min, dehydrated and embedded in Spurr's epoxy resin that was baked for 48 h at 60 °C. Thin sections (70–90 nm) were obtained with a Leica EM UC6 ultramicrotome (Leica Microsystems, Austria), stained with a saturated solution of uranyl acetate in ethanol 20% and 1% lead citrate. Grids were observed in a Philips CM10 TEM (FEI, Eindhoven, Netherland). The excitatory synapses that were included in the EM analyses were those fitting these 3 criteria: (1) presence of a cluster of presynaptic vesicles (at least 3 of them); (2) presence of a defined synaptic cleft; and (3) presence of the postsynaptic density (Burette et al. 2015). For quantitative analyses, images were acquired at a final magnification of ×25.000–34.000 using a Morada CDD camera (Olympus, Munster, Germany). Quantitative measurements were performed with ImageJ 1.47 v.

### Serial Block Face Scanning Electron Microscopy— Sample Preparation, Image Acquisition and Analyses

Tissue fixation and embedding were performed as described (Denk and Horstmann 2004) with slight modifications.

Serial block-face (SBF) datasets were collected using a FEI Quanta 200 F SEM, equipped with a Schottky field emission electron source, operating at an accelerating voltage of 3 kV, with beam current of 21 pA in a water low pressure of 30 Pa, and by using a Gatan 3View SBF-system (Gatan, Pleasanton, CA, USA).

The resulting datasets were assembled into volume files aligned using Digital Micrograph (Gatan), and then manually

segmented into 3-dimensional (3D) models in AMIRA 5.4.3 software package (FEI Visualization Science Group, Burlington, MA, USA). 3D structures in image stacks containing hundred or thousand of 2D orthoslices were traced individually in each plane and automatically surface rendered. The volumes of Amira 3D models were measured by the 'Material Statistics' tool.

## SDS-Page and Immunoblotting

Analysis of synaptic markers was performed on hippocampal lysates from 90 days old male $Tm4sf2^{+/y}$ and $Tm4sf2^{-/y}$ mice. Hippocampi were homogenized in modified RIPA buffer (20 mM Tris, 150 mM NaCl, 1 mM EDTA, 1% NP40, 1% Triton X-100, protease inhibitors cocktail) and centrifuged $9000 \times g$ 4 °C for 30 min. Collected supernatants were quantified and consequently analyzed by SDS-PAGE and Western blot. Antibodies were diluted in blocking buffer (5% non-fat dry milk in TBST 0.1%) (Supplementary Table 1).

## BS3 Crosslinking

The experiments were carried out as previously described (Folci et al. 2016) and in parallel with electrophysiology. Briefly, mice were sacrificed, and brain slices of 400 μm thickness were cut using a vibratome and rapidly put in ice-cold artificial cerebral spinal fluid (aCSF). Cell membrane impermeable BS3 crosslinker (PierceNet) was prepared as a 52 mM stock in 5 mM sodium citrate buffer pH 5. The slices were then put into a 12-well plate with 1 ml of ice-cold aCSF and BS3 added to a final concentration of 2 mM. The plate was incubated for 30 min at 4 °C with gentle agitation. Glycine was added to a final concentration of 100 mM and incubated for 10 min at 4 °C with gentle agitation to quench the reaction. The slices were then collected and lysed with mechanical homogenization in lysis buffer (50 mM Tris, 150 mM NaCl, 1 mM EDTA, 1% SDS, pH 7.4). The lysates were then loaded on acrylamide gel and underwent standard western blotting procedures to analyze GluA2, GluA2/3, GluA1, α-tubulin, and transferrin receptor expression.

## Electrophysiology

Coronal hippocampal slices (thickness, 250–400 μm) from C57Bl/6 $Tm4sf2^{+/y}$ and $Tm4sf2^{-/y}$ 60 days old male mice were prepared as previously described (Folci et al. 2016).

Miniature AMPA (AMPA-mEPSCs) and evoked excitatory postsynaptic currents (eEPSCs) were recorded at a holding potential of –65 mV with an internal solution containing (in mM) 126 K-gluconate, 4 NaCl, 1 EGTA, 1 MgSO$_4$, 0.5 CaCl$_2$, 3 ATP (magnesium salt), 0.1 GTP (sodium salt), 10 glucose, and 10 HEPES-KOH (pH 7.28). Access resistance was between 10 and 20 MΩ; if it changed by > 20% during the recording, the recording was discarded.

All glutamatergic currents were recorded in the presence of the GABA$_A$ blocker bicuculline (20 μM) in the aCSF. For the recording of AMPA-mEPSCs, lidocaine (500 μM), and the NMDA blocker APV (100 μM) were added to the aCSF. Hippocampal CA1 pyramidal neurons eEPSCs were elicited stimulating the Schaffer collaterals (SC) with a patch pipette placed near the patched neuron in the CA1.

For AMPAR rectification experiments eEPSCs were recorded using a cesium chloride-based intracellular solution consisting of (in mM) 140 CsCl, 2 MgCl$_2$, 1 CaCl$_2$, 10 EGTA, 10 HEPES-CsOH, 2 ATP (disodium salt), 0.15 spermine (pH 7.3) and adding to the aCSF bicuculline (20 μM) and APV (100 μM) to isolate AMPARs-mediated currents. The RI was identified by the ratio between the amplitude of the currents recorded at –60 mV and the currents recorded at +40 mV. Paired pulse experiments were performed and analysed as described (Folci et al. 2016).

Miniature inhibitory postsynaptic currents (mIPSCs) and current clamp analyses were performed as previously described (Pizzamiglio et al. 2016). Currents through the patch-clamp amplifier were filtered at 2 kHz and digitized at 20 kHz using Clampex 10.1 software.

fEPSPs were evoked (0.05 Hz of frequency) and recorded from the *stratum radiatum* of the hippocampal CA1 stimulating the SC using aCSF-filled monopolar glass electrodes. fEPSPs were acquired at 20 kHz and filtered at 5 kHz. Input–output (I–O) curves were constructed by measuring the slope of fEPSPs evoked in response to stimulation with increasing intensity (0–1.0 mA). Stimulus strength was adjusted to give 50% maximal response and long-term potentiation (LTP) was elicited using 2 protocols: the first one consisting of 100 stimuli at 100 Hz and the second one, much stronger, consisting of 100 stimuli at 250 Hz. All the analyses were performed offline with Clampfit 10.1 software.

## Behavioral Tests

All behavioral tests were performed on 90 days old male mice. Animals were maintained on a 12 h light cycle (lights on at 8.00 AM) with exception for light and dark (L/D), emergence and fear conditioning tests where mice were maintained on an inverse 12 h light and dark cycle (lights on from 8.00 PM). In this case the experiments were carried out during the dark phase of the cycle.

Food pellets and water were available ad libitum if not stated otherwise.

L/D, emergence and fear conditioning tests were performed according to the animal protocols approved by the Institutional Animal Care and Use Committee San Raffaele (IACUC) (San Raffaele, Milan, Italy) and approved by the National Ministry of Health (IACUC ID 653).

Animals were video-tracked using the EthoVision 2.3 system (Noldus Information Technology, Wageningen, the Netherlands, ://www.noldus.com) using an image frequency of 4.2/s. Raw data were transferred to Wintrack 2.4 (http://www.dpwolfer.ch/wintrack) for offline analysis. During Fear conditioning tests, animals were continuously video-tracked using the ANY-maze system (Anymaze, Stoelting Co, Wood Dale, IL, USA, www.anymaze.com). The frequency of freezing (absence of movements except respiration) was continuously recorded.

For all tests statistical computations were done using Statview 5.0 (SAS Institute, Cary, NC, USA, www.statview.com)

## Light and Dark Test

The experiment was performed on a $20 \times 30$ cm$^2$ lit chamber with transparent Perspex walls (20 cm high) and open top was connected to a $20 \times 15 \times 20$ cm$^3$ plastic dark box which was completely closed except for the $7.5 \times 7.5$ cm$^2$ door connecting it to the lit chamber. Illumination was by direct room light (500 lx). Each mouse was released in the middle of the lit compartment and observed for 5 min.

## Emergence Test

Frames of non-reflective black Perspex walls (37 cm high) were used to partition a round open field arena (diameter of 150 cm

and 35-cm high walls) into 4 squares (50 × 50-cm$^2$ arena), allowing for concurrent tracking of 4 animals at one time. The day before this test a box made of plastic (12 × 8 × 4 cm$^3$ with a door of 8 × 4 cm$^2$) was inserted in each mouse's home cage. The same box was then placed in a corner of the arena, with the opening facing the center of the arena. The mice were released into the center of the arena and tracked for 30 min. Illumination in the room was provided by indirect diffuse light (4 × 40-W bulbs, 12 lx).

## Spontaneous Motor Activity

Spontaneous motor activity was evaluated in an automated activity cage (43×43×32 cm$^3$) (Ugo Basile, Varese, Italy), placed in a sound-attenuated room. The cage was fitted with 2 parallel horizontal and vertical infrared beams located 2.5 and 5 cm from the floor, respectively. Horizontal and vertical beam breaks were counted, every 10 min, for 120 min. After treatment with CX516 animals were tested only for 30 min.

## Swimming Speed

Swimming speed was monitored as previously described (Folci et al. 2016).

## Novel Object Recognition

The test was carried out over a two-day period in an open plastic arena (60 cm × 50 cm × 30 cm) as previously described (Pan et al. 2008). Animals were habituated to the test arena for 10 min on the first day and then were subjected to familiarization (T1) and novel object recognition (T2). During the initial familiarization stage, 2 identical objects were placed in the center of the arena equidistant from the walls and from each other. Each mouse was placed in the center of the arena between the 2 objects for a maximum of 20 min or until it had completed 30 s of cumulative object exploration. Object recognition was scored when the animal was within 0.5 cm of an object with its nose toward the object. Exploration was not scored if a mouse reared above the object with its nose in the air or climbed on an object. Mice were returned to the home cage after familiarization and then tested again after different delays (5 min, 120 min, and 24 h later). A novel object (never seen before) took the place of 1 of the 2 familiars.

Scoring of object recognition was performed in the same manner as during the familiarization phase. From mouse to mouse the role (familiar or new object) as well as the relative position of the 2 objects were counterbalanced and randomly permuted. The objects for mice to discriminate consisted of white plastic cylinders and colored plastic Lego stacks of different shape. The arena was cleaned with 70% ethanol after each trial. An experimenter blind to the genotype group manually recorded the exploration times to the objects for each animal. Total time spent to exploring the 2 objects during T1 and T2 was also calculated.

## Spatial Object Recognition

For the spatial object recognition the animals were first habituated to test apparatus for 10 min for one day. Then they were subjected to a familiarization trial (T1) and a spatial object recognition trial (T2) with a delay of 5 min or 120 min, or 24 h from T1. During T1 and T2 mice were placed into the open field arena for a maximum of 20 min or until it had completed 30 s of cumulative object exploration and allowed to explore 2

different objects. In T1, 2 different objects were placed in NE and NW corners, approximately 5 cm from the walls of the open field arena. Then the mice were returned in the home cage. After 5 min, 120 min, or 24 h mice were re-exposed to the open field arena with the more explored object moved toward the opposite side of the test arena. Mice will preferentially explore a spatially displaced object than one remained stationary. Objects were counterbalanced across locations and conditions. The open field arena and all objects were thoroughly wiped down with 70% ethanol before and after all behavioral procedures. Care was taken to minimize the difference between the to-be discriminated objects in order to prevent a greater preference for one of the 2 objects. An experimenter blind to the treatment group manually recorded the exploration times to the objects in each animal. Mice that did not explore any of the 2 objects/shapes for at least 30 s during T1 were excluded from the data analysis. The basic measure for all the object tests was the time mice spent in exploring each object/shape during T1 and T2. The discrimination index ([time spent exploring novel object−time exploring familiar object]/[time spent exploring novel object + time exploring familiar object]) was calculated as described elsewhere (Pitsikas et al. 2001). The rescue with CX516 was evaluated only after a delay of 24 h between T1 and T2.

## Water Maze

To evaluate the integrity of hippocampus-dependent memory formation in $Tm4sf2^{+/y}$ and $Tm4sf2^{-/y}$ mice, the water maze paradigm according to Morris et al. (1982) (Morris et al. 1982), was used. Water maze was a circular tank (diameter 1.5 m) filled with water (25 °C ± 0.5 °C). A platform (13.5 cm × 23 cm) was submerged below the water's surface in the center of the target zone. Floating polystyrene particles were placed on the surface of the water to hide the platform from sight. Extra maze cues (simple geometrical shapes) and visual references (chair, table) were present around the room to provide spatially oriented cues. Four points around the circumference of the maze were arbitrarily designated as N, S, E, and W, which served as a reference for experimenters when releasing the mice into the pool. For the acquisition trial, mice performed 4 trials per day (with 60 s of intertrial interval) for 4 consecutive days in which each mouse was released to the pool from different starting points and trained to a constant platform position. 24 h after the last trial a probe test was carried out during which the platform was removed. Two days after, a reversal task was performed in order to assess cognitive flexibility. The platform was placed in the opposite quadrant in the tank and there were 4 daily trials for 4 days. And 24 h later, a probe trial was given similar to that of acquisition phase. An experimenter, blind to the genotype, manually recorded the escape latency during training phase and the latency and the time spent in the target zone of the maze during probe phase. After each trial, mice were placed on a paper towel for additional drying and then put back into their home cages.

## Trace and Standard Fear Conditioning

Auditory trace and delay fear conditioning were performed by placing the mice in an opaque conditioning chamber (L × W × H: 25 × 17 × 23 cm$^3$) with a grid floor through which scrambled foot shocks could be delivered as unconditioned stimuli (US; 0.26 mA average intensity). The chamber was placed into a dimly lit (<5 lux) sound attenuating box (background noise level

55 dB), and a speaker on top of the chamber allowed to deliver sounds as conditioning stimuli (CS; 2000 Hz).

All mice were pre-exposed to the test chamber for 10 min on the day preceding conditioning. On day 2, the day of the conditioning, after 60s of baseline period (no stimulus), 5 trials were presented separated by 60 s of intertrial intervals (ITI). In the trace fear conditioning, every trial is composed by the presentation of the CS (15 s) followed, 15 s later, by the presentation of the shock for 2 s. Instead in the delay fear conditioning each trial is composed by the CS (15 s), with the US delivered during the last 2 s of CS presentation.

The mice freezing behavior was measured during the presentation of the CS. And 24 h after fear conditioning, mice were placed in the conditioning box again, measuring their freezing behavior in the context test and tone test. Context testing consisted of 2 min without CS ("contextual freezing"), tone testing consisted of 1 min without CS followed by 1 min with the CS turned on.

### Pep2-SVKE and Pep2-EVKI Mice Treatment

To interfere with PICK1 we treated $Tm4sf2^{+/y}$ and $Tm4sf2^{-/y}$ 60 days old male mice by intraperitoneal injection (i.p.) of TAT-fused active (pep2-EVKI) or inactive (pep2-SVKE) peptides (ChinaPeptides Co., Ltd.) (both at 3 μmol kg$^{-1}$) 15 h before the slice procedure, as previously described (Bellone and Luscher 2006).

### CX516 Chronic Treatment

The 60–90 days old male mice, housed in groups of maximum 4 per home cage and maintained on a 12 h light/dark cycle with food and water ad libitum, were treated as described (Baudry et al. 2012). Briefly, $Tm4sf2^{+/y}$ and $Tm4sf2^{-/y}$ mice received 2 i.p. injections per day, at 8:00–9:00 AM and 5:00–6:00 PM, for a total of 8 days. For the first 3 days, mice were treated with vehicle injections of saline plus 15–20% 2-hydroxypropyl-beta-cyclodextrin (Sigma). After this habituation period, mice assigned to drug treatment were injected for the next 5 days with the ampakine CX516 (5 mg/kg) (Sigma), whereas control-assigned mice continued to receive vehicle injections. Mice received the last i.p. injection 15 h before the experiments.

### Data Analysis

All data are presented as mean ± S.E.M (standard error of the mean). Significance was taken at $P < 0.05$ using unpaired Student's $t$-test, or one- or two-way ANOVA with multiple-comparison test, as applicable. The use of the paired Student's $t$-test and two-way ANOVA for repeated measures are stated in the main text or in Supplementary Tables. Statistical comparisons are stated in results or in Supplementary Tables.

## Results

### Absence of TSPAN7 Alters the Postsynaptic Compartment of Excitatory Synapses in the CA1 Region of the Hippocampus

To examine TSPAN7 function in vivo, we generated $Tm4sf2$-knockout ($Tm4sf2^{-/y}$) mice (Supplementary Fig. 1A). Western blot analysis confirmed the absence of TSPAN7 protein (27 kDa) in the brains of the mutant mice (Supplementary Fig. 1B). Histological analysis was performed on sections of paraffin-embedded brain tissue and showed no changes in the brain structure neither in hippocampi nor in cortex architecture in

either young (P30) or adult (P90) $Tm4sf2^{-/y}$ mice compared with $Tm4sf2^{+/y}$ mice (data not shown and Supplementary Fig. 1C). Therefore we initially concentrated on the hippocampus considering its role in learning and memory, which are the cognitive functions mainly impaired in patients with mutations in $TM4SF2$, and the results obtained in hippocampal culture neurons (Bassani et al. 2012). Ultrastructural analysis of excitatory synapses revealed a significant reduction in the length and thickness of postsynaptic densities (PSDs) (Dosemeci et al. 2001) in both young (Supplementary Fig. 1D) and adult $Tm4sf2^{-/y}$ mice (Fig. 1A and Supplementary Table 2). To support these observations deriving from two-dimensional projections, we processed tissue blocks from the apical dendrite layer of the hippocampal CA1 region for serial block-face scanning electron microscopy (SBFSEM) and 3D volume reconstruction. From the stack of serial aligned images, volumes were reconstructed, and structures of interest (PSDs, dendritic spines and dendrites) were segmented, modeled and measured using AMIRA software. Consistent with the PSD reductions observed in the hippocampal sections from adult $Tm4sf2^{-/y}$ mice, we observed a significant reduction in PSD volume in the corresponding samples (Fig. 1B and Supplementary Table 2). Lack of TSPAN7 specifically affected PSD, while the volume of spine heads was unaffected (Fig. 1B and Supplementary Table 2).

Finally, we used SBFSEM series reconstruction (total of 500 μm$^3$ of hippocampal tissue) to evaluate differences in spine density between $Tm4sf2^{+/y}$ and $Tm4sf2^{-/y}$ mice in the apical dendrites of the CA1 region. In young animals, there was no difference in spine density in the apical dendrites of the CA1 region between genotypes (Supplementary Fig. 1D), whereas the spine density was significantly reduced in the CA1 region of adult $Tm4sf2^{-/y}$ mice compared with control mice (Fig. 1B and Supplementary Table 2). This difference between young and adult mice could be due to the fact that young animals have more plastic spines that undergo faster turnover than adult animals, which have remarkably stable spines (Grutzendler et al. 2002). To determine whether $Tm4sf2$ ablation exclusively affects the postsynaptic compartment or more generally affects asymmetric synapses, we performed quantitative measurements of excitatory presynaptic terminals in the hippocampal CA1 regions of $Tm4sf2^{+/y}$ and $Tm4sf2^{-/y}$ mice. Once differences in individual synaptic vesicles were excluded (Supplementary Table 2), we measured the presynaptic profile, synaptic vesicle density and vesicle distribution inside synaptic terminals. Regardless of mouse genotype or age, all these parameters were similar among the examined samples (Fig. 1A and Supplementary Table 2; Supplementary Fig. 1D).

We found that $Tm4sf2$ gene disruption had no effect on the structure of inhibitory synapses within the same hippocampal region. Inhibitory synaptic profiles were identified on thin sections based on positive staining with antibodies against the neurotransmitter GABA (Supplementary Fig. 2A). In these profiles, we measured the mean presynaptic surface and synaptic vesicle density. The absence of TSPAN7 had no effect on the structure of inhibitory terminals (Supplementary Fig. 2B).

Next, we used western blotting to determine how lack of TSPAN7 expression changes the levels of endogenous pre- and postsynaptic proteins in the hippocampus. The results showed a significant reduction in the expression of the GluA2 and GluA2/3 AMPAR subunits (GluA2: $Tm4sf2^{+/y}$ 1.000 ± 0.049 vs. $Tm4sf2^{-/y}$ 0.640 ± 0.043, **$P < 0.01$; GluA2/3: $Tm4sf2^{+/y}$ 1.000 ± 0.032 vs. $Tm4sf2^{-/y}$ 0.700 ± 0.027, unpaired $t$-test **$P < 0.01$. At least 6 mice per genotype were analysed). By contrast, GluA1, PSD95, Gephyrin, Neuroligin 2, PICK1, the α1 subunit of
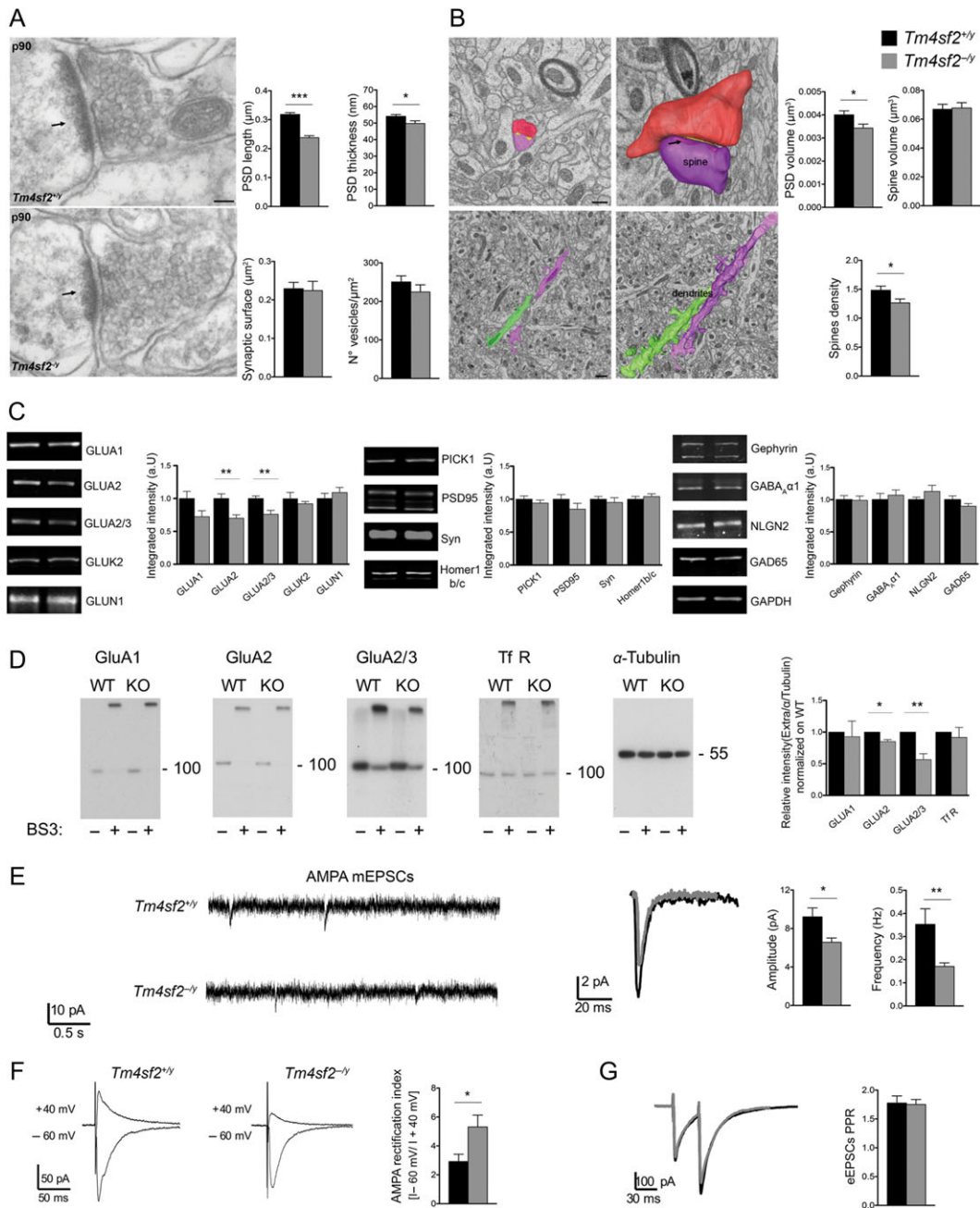
**Figure 1.** *Tm4sf2* loss of function alters structure and function of hippocampal excitatory synapses. (A) Electron micrographs of asymmetrical synapses of the *stratum radiatum* of the hippocampal CA1 regions of *Tm4sf2*[+/y] and *Tm4sf2*[−/y] mice. The postsynaptic density is indicated with the arrows. Scale bar, 50 nm. The mean length and thickness of the PSDs, presynaptic mean surface and vesicle density were evaluated in *Tm4sf2*[+/y] and *Tm4sf2*[−/y] adult mice. (B, upper panel) Representative section and 3D reconstruction of the head of a dendritic spine (purple), the PSD (yellow) and the presynaptic bouton (red) from a 35 μm³ volumetric data-set containing 28 serial images of a mouse CA1 region. Scale bar, 500 nm. (B, lower panel) Representative section (left) and 3D reconstruction of dendrites (right) from a 518 μm³ volumetric data-set containing 46 serial images of hippocampal CA1 region. Scale bar, 1 μm. PSD volume, spine head volume and spine density were evaluated in *Tm4sf2*[+/y] and *Tm4sf2*[−/y] adult mice. (C) Western blots of hippocampal homogenates from *Tm4sf2*[+/y] and *Tm4sf2*[−/y] mice detected using LI COR technology and quantification of synaptic protein levels. *Tm4sf2*[−/y] mice had lower levels of GluA2 and GluA2/3 compared with *Tm4sf2*[+/y] mice, while all other postsynaptic and presynaptic markers were similar between genotypes. (D) Western blots from BS3 crosslinking experiments on mouse brain slices to detect surface AMPAR pools. Both high (surface expressed) and predicted (intracellular) molecular weight bands were detected in tissue treated with the crosslinker (BS3+), whereas surface proteins from untreated tissues (BS3−) and intracellular proteins (tubulin) yielded single bands. Quantifications of surface/tubulin AMPAR subunits normalized to *Tm4sf2*[+/y] are shown. In *Tm4sf2*[−/y] mice, the surface GluA2 and GluA2/3 levels were reduced with respect to *Tm4sf2*[+/y] mice, whereas GluA1 and transferrin receptor (TfR) levels were unaffected. (E) Representative traces and quantification of *Tm4sf2*[+/y] and *Tm4sf2*[−/y] mice AMPAR-mEPSC amplitude and frequency recorded from hippocampal CA1 pyramidal neurons. (F) Representative traces of AMPA currents recorded at −60 mV and +40 mV from CA1 pyramidal neurons and quantification of the AMPARs rectification index (RI) from *Tm4sf2*[+/y] and *Tm4sf2*[−/y] mice. (G) Paired pulse ratio experiments showed no difference for glutamate release probability between genotypes. Statistical comparison are stated in the main text or in Supplementary Table 2.

GABA$_A$R, GluN1, GluK2, Homer and the presynaptic markers Synaptophysin and GAD65 were unaltered (Fig. 1C). Next, we determined whether a decrease in AMPAR subunit expression occurred at the neuron cell surface. BS3 crosslinking experiments were used to quantify the surface expression of membrane proteins, and the results showed that $Tm4sf2^{-/y}$ mice displayed lower levels of GluA2 and GluA2/3-containing AMPAR at the plasma membrane than $Tm4sf2^{+/y}$ mice (GluA2: $Tm4sf2^{+/y}$ $1 \pm 0$ vs. $Tm4sf2^{-/y}$ $0.85 \pm 0.03$, *$P < 0.05$; GluA2/3: $Tm4sf2^{+/y}$ $1 \pm 0$ vs. $Tm4sf2^{-/y}$ $0.57 \pm 0.09$, **$P < 0.01$, unpaired $t$-test.) (Fig. 1D). By contrast, the surface expression of the GluA1 subunit and the transferrin receptor was unaltered (Fig. 1D). These findings are consistent with the observed reductions in PSD size and spine number in the $Tm4sf2^{-/y}$ mice.

## $Tm4sf2$ Loss of Function Impairs Hippocampal Excitatory Transmission at Schaffer Collateral-CA1 Synapses

To explore the physiological consequences of the structural modifications induced by $Tm4sf2$ loss of function, we investigated basal synaptic transmission in the Schaffer collateral (SC)–CA1 pathway in hippocampal slices from $Tm4sf2^{+/y}$ and $Tm4sf2^{-/y}$ mice.

We found that $Tm4sf2$ loss of function induced changes in the basal properties of AMPAR-mediated miniature excitatory postsynaptic currents (AMPAR-mEPSCs) compared with wild-type mice (Amplitude: $Tm4sf2^{+/y}$ $n_{cells} = 7$: $9.2 \pm 0.9$ pA vs. $Tm4sf2^{-/y}$ $n_{cells} = 10$: $6.6 \pm 0.4$ pA; *$P < 0.05$ unpaired $t$-test; and frequency: $Tm4sf2^{+/y}$ $n_{cells} = 7$: $0.35 \pm 0.07$ Hz vs. $Tm4sf2^{-/y}$ $n_{cells} = 10$: $0.17 \pm 0.02$ Hz; **$P < 0.01$ unpaired $t$-test). Notably, $Tm4sf2^{-/y}$ mice showed significant reduction in the amplitude and frequency of AMPAR-mEPSCs (Fig. 1E). It has been well established that mEPSC amplitude is directly linked to postsynaptic function and that changes in this parameter are associated to changes in postsynaptic receptor efficacy and/or density. In the present study, the observed decrease in amplitude was in agreement with the reduced expression levels of the GluA2 and GluA2/3 AMPAR subunits. Furthermore, $Tm4sf2^{-/y}$ mice showed an increased AMPAR RI relative to $Tm4sf2^{+/y}$ mice ($Tm4sf2^{+/y}$ $n_{cells} = 7$: $2.9 \pm 0.5$ vs. $Tm4sf2^{-/y}$ $n_{cells} = 6$: $5.3 \pm 0.8$; *$P < 0.05$ unpaired $t$-test) (Fig. 1F). AMPAR RI, calculated as the ratio between the current evoked at negative potential and the current evoked at positive potentials, is routinely used as a readout for modification in AMPARs subunit composition, taking advantage of the different channel conductance that GluA2 AMPAR subunit confers to the receptor. In particular, it is widely reported that GluA2-lacking AMPARs are more rectifying compared with GluA2-containing AMPARs (Adesnik and Nicoll 2007; Derkach et al. 2007). With our experiments, we showed that AMPAR RI was increased in $Tm4sf2^{-/y}$ mice compared with $Tm4sf2^{+/y}$ mice reinforcing the evidence of a decreased number of GluA2-containing AMPARs in $Tm4sf2^{-/y}$ mice (Washburn et al. 1997; Jackson and Nicoll 2011).

To further explore the effect of the absence of TSPAN7 on AMPA-mEPSC frequency, we performed paired pulse ratio (PPR) experiments to analyse the ratio between the second and first evoked response in $Tm4sf2^{+/y}$ and $Tm4sf2^{-/y}$ mice. The results showed no significant difference in neurotransmitter release probability between genotypes (Fig. 1G), indicating that the reduction in AMPA-mEPSC frequency resulted either from the presence of under-threshold currents masked by background noise or a reduced number of functional synapses caused by the observed reduction in spine density. $Tm4sf2$ loss of function

had no effect on the basal properties of GABA-mediated miniature inhibitory postsynaptic currents (GABA-mIPSCs) compared with $Tm4sf2^{+/y}$ mice (Supplementary Fig. 2C, D).

To assess whether $Tm4sf2$ disruption could affect the excitation-inhibition balance in the brain, we measured the excitability in brain slices from CA1 hippocampal pyramidal neurons from $Tm4sf2^{-/y}$ and $Tm4sf2^{+/y}$ mice. After the application of somatic depolarizing current stimuli, we evaluated action potential (AP) firing properties analysing parameters usually associated to neuronal excitability such as AP threshold, minimum current intensity (MCI) and AP firing frequency (Pizzamiglio et al. 2016). AP threshold is defined as the membrane voltage at which AP firing starts, while the MCI is the current that has to be injected inside neurons to reach the threshold for AP. In presence of an unbalance between excitation and inhibition these parameters result altered. In particular, when the inhibition is prominent, as for example upon exaggerated GABAergic or decreased glutamatergic transmission, the threshold for AP results increased as well as more current has to be injected to reach the new threshold for AP. We showed that $Tm4sf2^{-/y}$ mice resulted to be impaired for AP threshold, MCI and AP firing frequency (AP threshold: $Tm4sf2^{+/y}$ $n_{cells} = 27$: $-51.3 \pm 0.9$ mV vs. $Tm4sf2^{-/y}$ $n_{cells} = 21$: $-47.8 \pm 1.3$ mV, unpaired $t$-test *$P < 0.05$; MCI: $Tm4sf2^{+/y}$ $n_{cells} = 27$: $36.7 \pm 4.7$ pA vs. $Tm4sf2^{-/y}$ $n_{cells} = 20$: $83.0 \pm 10.5$, unpaired $t$-test ***$P < 0.0001$; AP frequency: $Tm4sf2^{+/y}$ $n_{cells} = 28$ vs. $Tm4sf2^{-/y}$ $n_{cells} = 19$ two-way ANOVA RM, $f_{1-225} = 15.92$, ***$P < 0.001$) (Fig. 2A). Altogether, these results indicate that $Tm4sf2$ loss of function negatively modulates excitatory transmission and that hippocampal pyramidal neurons are less excitable in $Tm4sf2^{-/y}$ mice than in $Tm4sf2^{+/y}$ mice.

## Long-term Potentiation is Altered in $Tm4sf2^{-/y}$ Mice

Next, we examined whether the above alterations affected synaptic plasticity in $Tm4sf2^{-/y}$ mice. To accomplish this, we recorded field excitatory postsynaptic potentials (fEPSPs) (Fig. 2B) to study basal hippocampal synaptic activity and LTP in $Tm4sf2^{-/y}$ and $Tm4sf2^{+/y}$ mice.

First, we stimulated SC with increasing intensity (0–1.0 mA) to generate input/output (I/O) curves. Then, we recorded fEPSPs from the *stratum radiatum* of the CA1 region and evaluated changes in fEPSP slopes as a percentage of the maximal response. The results showed that $Tm4sf2^{-/y}$ mice have smaller evoked responses than wild-type mice, suggesting that these mice have weaker SC-CA1 synapses than $Tm4sf2^{+/y}$ mice ($Tm4sf2^{+/y}$ $n_{slices} = 5$ vs. $Tm4sf2^{-/y}$ $n_{slices} = 6$, two-way ANOVA RM with Bonferroni post hoc test, $f_{1-90} = 5.66$, *$P < 0.05$, **$P < 0.01$) (Fig. 2C). PPR experiments using the field potential configuration confirmed that there were no significant differences in the glutamate release probability between the genotypes (Fig. 2D). Next, we recorded fEPSPs at SC-CA1 synapses before and after NMDA-dependent LTP induction, using 10 min of recording of a half-maximal response as the baseline. Notably, LTP induction at the SC-CA1 synapse was severely impaired in $Tm4sf2^{-/y}$ mice compared with control animals (Fig. 2 E and Supplementary Fig. 3A). By contrast, when we removed $Mg^{2+}$ from the aCSF, we observed normal LTPs even in $Tm4sf2^{-/y}$ mice ($Tm4sf2^{+/y}$ $n_{slices} = 9$: $203.8 \pm 20.6\%$ vs. $Tm4sf2^{-/y}$ $n_{slices} = 5$: $115.4 \pm 17.3\%$ vs. $Tm4sf2^{-/y}$ $Mg^{2+}$ free $n_{slices} = 5$: $185.2 \pm 16.6\%$, *$P < 0.05$ one-way ANOVA followed by Newman–Keuls post test) (Fig. 2E), suggesting that AMPAR cannot induce the removal of $Mg^{2+}$ from NMDAR and thus prevents the induction of LTP.
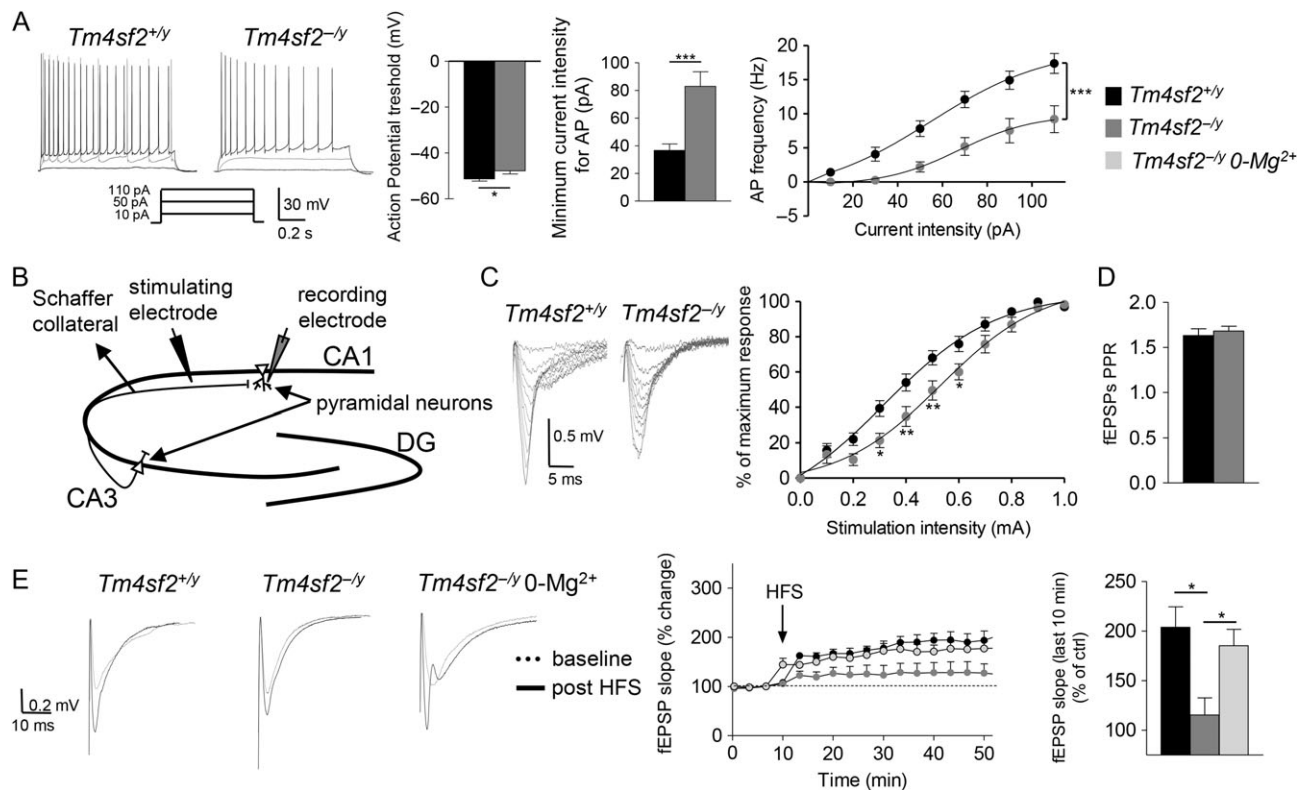
**Figure 2.** *Tm4sf2* loss of function alters neuronal excitability and long-term synaptic plasticity. (A) Representative traces of current clamp experiments and analysis of AP threshold, MCI and AP frequency in *Tm4sf2*+/y and *Tm4sf2*−/y mice. (B) Scheme of fEPSP recordings showing the placement of the stimulating and recording electrodes. (C) Representative traces of fEPSPs and the I/O relationship in *Tm4sf2*+/y and *Tm4sf2*−/y mice. (D) fEPSP paired pulse experiment confirmed no differences in glutamate release. (E) fEPSP representative traces and quantification of LTP experiments (100 stimuli at 250 Hz) showing LTP impairment in *Tm4sf2*−/y mice, which was recovered by removing Mg$^{2+}$ before conditioning. All data are represented as the mean ± S.E.M. Statistical comparison are stated in the main text.

Overall, these results suggest that TSPAN7 has a role in excitatory synaptic transmission and plasticity in the hippocampus.

## *Tm4sf2*−/y Mice Have Defects in Hippocampal-Dependent Episodic, Spatial and Associative Memory

We monitored *Tm4sf2*−/y and *Tm4sf2*+/y littermates to examine their explorative and emotional behaviors using a dark/light box, emergence tests and activity cages. The results showed no differences between the genotypes and indicated that both had intact explorative and emotional behaviors (data not shown).

Next, episodic and spatial memory was tested in *Tm4sf2*−/y and *Tm4sf2*+/y mice using novel object recognition, spatial object recognition and water maze tests.

In the novel object recognition task, *Tm4sf2*−/y mice showed a reduced discrimination index when tested 5 min, 120 min and 24 h after familiarization compared with *Tm4sf2*+/y mice [5 min delay: *Tm4sf2*+/y: 0.1329 ± 0.0300 vs. *Tm4sf2*−/y: −0.0814 ± 0.0300; 120 min delay: *Tm4sf2*+/y: 0.2571 ± 0.0416 vs. *Tm4sf2*−/y: −0.1557 ± 0.0300; 24 h delay: *Tm4sf2*+/y: 0.27 ± 0.04 vs. *Tm4sf2*−/y: −0.03 ± 0.04; $n_{mice}$ = 7 per group, **$P < 0.01$, ***$P < 0.001$, two-way ANOVA showed difference in the genotype ($F_{1,36}$ = 27.30, $P < 0.0001$) in the time ($F_{2,36}$ = 11.17, $P < 0.001$) but not in the interaction genotype × time ($F_{2,36}$ = 1.927, $P > 0.05$)] (Fig. 3A). The mean exploration time to the novel object was increased in *Tm4sf2*+/y mice compared with the familiar in all tested intervals, while *Tm4sf2*−/y mice showed no difference in mean exploration time between familiar and novel object (Supplementary Fig. 4A). This result suggests that the *Tm4sf2*−/y mice had defects in recognition

memory, which agrees with a previous report that damage to the hippocampus is sufficient to impair recognition memory (Squire et al. 2007). In the spatial object recognition task, *Tm4sf2*+/y mice preferentially explored the spatially displaced object compared with the object that remained stationary during the recognition trial, whereas *Tm4sf2*−/y mice spent the same amount of time exploring both objects [5 min delay: *Tm4sf2*+/y: 0.2475 ± 0.0497 vs. *Tm4sf2*−/y: −0.1333 ± 0.0375; 120 min delay: *Tm4sf2*+/y: 0.2467 ± 0.0959 vs. *Tm4sf2*−/y: −0.1825 ± 0.0335; 24 h delay: *Tm4sf2*+/y: 0.1333 ± 0.0375 vs. *Tm4sf2*−/y: −0.1120 ± 0.0533; $n_{mice}$ = 7 per group, **$P < 0.01$ two-way ANOVA revealed differences in the genotype ($F_{1,36}$ = 60.29, $P < 0.0001$) but not time ($F_{2,36}$ = 0.351, $P > 0.05$) as well as in interaction genotype × time ($F_{2,36}$ = 1.476, $P > 0.05$)] (Fig. 3B). *Tm4sf2*+/y mice spent more time exploring the displaced object in comparison with the stationary one during all tested intervals, while *Tm4sf2*−/y mice does not displayed preference for the displaced object (Supplementary Fig. 4B) suggesting that *Tm4sf2*−/y mice failed to discriminate between the 2 objects.

In the water maze (Fig. 3C), *Tm4sf2*−/y mice showed an increased latency in finding the platform during the acquisition phase. During the probe test, *Tm4sf2*−/y mice showed a higher latency to reach the target zone [two-way ANOVA genotype: ($F_{1,48}$ = 28.78, $P < 0.0001$), time: ($F_{3,48}$ = 9.997, $P < 0.0001$) and genotype × time: ($F_{3,48}$ = 6.91, $P < 0.001$)] and spent less time in the target quadrant compared with *Tm4sf2*+/y mice (area under the curve (AUC): *Tm4sf2*+/y: 185.8 ± 12.07 vs. *Tm4sf2*−/y: 287.3 ± 27.62, $n_{mice}$ = 7 per group, unpaired t-test **$P < 0.01$) during training as well as showed a higher latency to reach the target zone (*Tm4sf2*+/y: 28.71 ± 7.517 vs. *Tm4sf2*−/y: 88.43 ± 16.17 $n_{mice}$ =
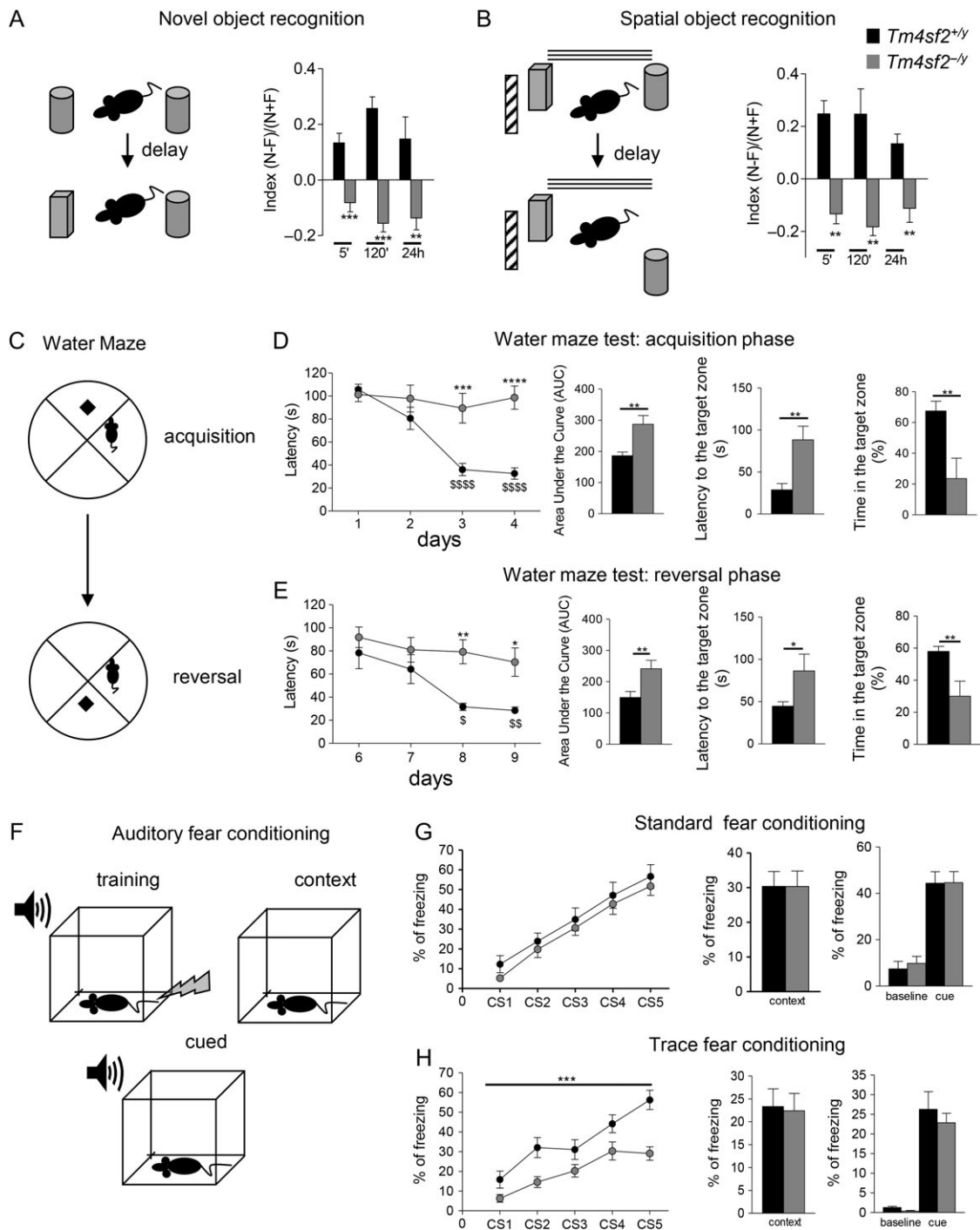
**Figure 3.** *Tm4sf2⁻/ʸ* mice display hippocampal-related behavioral impairments. (A) Novel object recognition test scheme and results: *Tm4sf2⁻/ʸ* mice showed reduced episodic memory in terms of discrimination index, evaluated after delays of 5 and 120 min and 24 h between T1 and T2. (B) Spatial object recognition test scheme and results: *Tm4sf2⁻/ʸ* mice showed impaired spatial memory evaluated in terms of reduced discrimination index after delays of 5 and 120 min and 24 h between T1 and T2. (C) Water maze test scheme. (D) Acquisition phase: *Tm4sf2⁻/ʸ* mice showed an increased latency to find the platform during the acquisition phase as well as a higher latency to reach the target zone, and they spent less time in this quadrant compared with *Tm4sf2⁺/ʸ* mice. (E) Water maze: reversal phase. *Tm4sf2⁻/ʸ* mice showed an increased latency to reach the platform and a higher latency to reach the target zone, and they spent less time in the quadrant that previously housed the platform compared with *Tm4sf2⁺/ʸ* mice. (F) Auditory fear conditioning test scheme. (G) Standard fear conditioning assessed in *Tm4sf2⁺/ʸ* and *Tm4sf2⁻/ʸ* mice showed no differences in acquisition phase or the cue test 24 hrs after the acquisition phase. (H) Trace fear conditioning assessed in *Tm4sf2⁺/ʸ* and *Tm4sf2⁻/ʸ* mice showed that the *Tm4sf2⁻/ʸ* mice exhibited impairments during the acquisition phase. No differences were observed when animals were tested for memory to the context 24 h later or in the tone test. All data are represented as the mean ± S.E.M. Statistical comparison are stated in the main text.

7 per group, unpaired *t*-test **P < 0.01) and spent less time in this quadrant compared with *Tm4sf2⁺/ʸ* mice in the test day (*Tm4sf2⁺/ʸ*: 67.48 ± 6.27 vs. *Tm4sf2⁻/ʸ*: 23.57 ± 13.24 n$_{mice}$ = 7 per

group, unpaired *t*-test **P < 0.01) (Fig. 3D). During the reversal phase, *Tm4sf2⁻/ʸ* mice took longer to find the target zone [two-way ANOVA genotype: ($F_{1,48}$ = 17.57, P < 0.0001), time: ($F_{3,48}$ =

5.19, $P < 0.01$) and genotype × time: ($F_{3,48} = 1.48$, $P > 0.05$)] and spent less time swimming in the quadrant that previously housed the platform than the $Tm4sf2^{+/y}$ mice (AUC: $Tm4sf2^{+/y}$: 149.4 ± 19.25 vs. $Tm4sf2^{-/y}$: 241.4 ± 26.94 $n_{mice} = 7$ per group, unpaired $t$-test **$P < 0.01$). In the probe trial of the reversal phase $Tm4sf2^{-/y}$ mice showed a higher latency to reach the target zone ($Tm4sf2^{+/y}$: 44.57 ± 5.205 vs. $Tm4sf2^{-/y}$: 86.25 ± 19.95 $n_{mice} = 7$ per group, unpaired $t$-test *$P < 0.05$) and spent less time in the quadrant that previously housed the platform compared with $Tm4sf2^{+/y}$ mice ($Tm4sf2^{+/y}$: 57.88 ± 3.18 vs. $Tm4sf2^{-/y}$: 30.01 ± 9.37, **$P < 0.01$ $n_{mice} = 7$ per group, unpaired $t$-test **$P < 0.01$) (Fig. 3E).

Finally the $Tm4sf2^{+/y}$ and $Tm4sf2^{-/y}$ mice were subjected to auditory fear conditioning, which measures mice associative learning. In this test, 2 procedures were used. Briefly, in the standard protocol, the unconditioned stimulus (US: foot shock) was superimposed for a short period of time with the presentation of the conditioned stimulus (CS: tone), while in trace fear conditioning protocol US presentation occurred a short while after the CS was presented and removed (Fig. 3F). Notably, trace and standard conditioning are dependent on different mechanisms, and only trace fear conditioning depends on an intact hippocampus (Huerta et al. 2000; Shors et al. 2000).

In the standard conditioning protocol, no significant differences between genotypes were found. Repeated presentation of the CS significantly elicited freezing in both groups (Fig. 3G), and no differences were observed during CS acquisition (ANOVA genotype effect: $F_{1,33} = 2.11$; $P > 0.05$), context (ANOVA genotype effect: $F_{1,33} = 0.01$; $P > 0.05$) or cue test (ANOVA genotype effect: $F_{1,33} = 0.15$; $P > 0.05$) (Fig. 3G). In contrast, in the trace fear conditioning protocol, $Tm4sf2^{-/y}$ mice showed significantly less freezing throughout the conditioning session compared with $Tm4sf2^{+/y}$ littermates (ANOVA genotype effect: $F_{1,37} = 20.5$; ***$P < 0.0001$) (Fig. 3H). These results suggested that $Tm4sf2^{-/y}$ mice are able to acquire fear-related behaviors but fail in retaining memory. No differences between genotypes were observed when animals were tested for context and cue test after 24 h (ANOVA genotype effect: $F_{1,37} = 0.8$; $P > 0.05$) or in the tone test (ANOVA genotype effect: $F_{1,37} = 0.5$; $P > 0.05$) (Fig. 3H). These data suggest that $Tm4sf2^{-/y}$ mice have impairments in spatial and associative memory.

## Rescue of Synaptic Impairment by pep2-EVKI Treatment in $Tm4sf2^{-/y}$ Mice

We previously demonstrated that TSPAN7 modulates GluA2 binding to the PICK1 PDZ domain and thereby regulates the internalization of GluA2-containing AMPAR (Bassani et al. 2012). This relationship prompted us to explore whether the application of a synthetic peptide that interferes with the PICK1 and GluA2 interaction (Bellone and Luscher 2006) could restore normal synaptic function in $Tm4sf2^{-/y}$ mice. To test this, $Tm4sf2^{+/y}$ and $Tm4sf2^{-/y}$ mice were treated with pep2-SVKE (inactive) and pep2-EVKI (active) peptides fused to an 11-amino-acid sequence derived from the Tat (48–57) protein of human immunodeficiency virus (HIV-1) to allow in vivo delivery into neurons (Fig. 4A). We found that pep2-EVKI, but not pep2-SVKE, increased the GluA2/3 surface expression ($Tm4sf2^{+/y}$+pep2-SVKE $n_{mice} = 4$: 1 ± 0 vs. $Tm4sf2^{-/y}$+pep2-SVKE $n_{mice} = 3$: 0.91 ± 0.01 vs. $Tm4sf2^{+/y}$+pep2-EVKI $n_{mice} = 3$: 1.85 ± 0.03 vs. $Tm4sf2^{-/y}$+pep2-EVKI $n_{mice} = 3$: 1.58 ± 0.07, *$P < 0.05$, ***$P < 0.001$ one-way ANOVA followed by Newman–Keuls post test) (Fig. 4B) and restored RI ($Tm4sf2^{+/y}$+pep2-SVKE $n_{cells} = 10$: 2.2 ± 0.3 vs. $Tm4sf2^{-/y}$+pep2-SVKE $n_{cells} = 12$: 4.7 ± 0.6 vs. $Tm4sf2^{+/y}$+pep2-

EVKI $n_{cells} = 7$: 2.4 ± 0.3 vs. $Tm4sf2^{-/y}$+pep2-EVKI $n_{cells} = 9$: 2.5 ± 0.2, **$P < 0.01$, one-way ANOVA followed by Newman–Keuls post test) in $Tm4sf2^{-/y}$ mice (Fig. 4C,D). We also found that treatment with pep2-EVKI recovered normal LTP in $Tm4sf2^{-/y}$ mice ($Tm4sf2^{+/y}$+pep2-SVKE $n_{slices} = 5$: 174.0 ± 20.5% vs. $Tm4sf2^{-/y}$+pep2-SVKE $n_{slices} = 8$: 115.2 ± 6.0% vs. $Tm4sf2^{+/y}$+pep2-EVKI $n_{slices} = 7$: 133.4 ± 11.0% vs. $Tm4sf2^{-/y}$+pep2-EVKI $n_{slices} = 6$: 167.3 ± 21.51%, *$P < 0.05$, one-way ANOVA followed by Newman–Keuls post test) (Fig. 4E, F). The disruption of PICK1–GluA2 binding slightly reduced the percentage of LTP in $Tm4sf2^{+/y}$ mice, in accordance with prior results (Terashima et al. 2008) (Fig. 4F). These data indicate that inhibiting the PICK1/GluA2 association leads to the complete recovery of synaptic plasticity in $Tm4sf2^{-/y}$ mice, likely due to decreased intracellular retention of AMPAR.

## Treatment With the Ampakine CX516 Rescues Synaptic Alterations in $Tm4sf2^{-/y}$ Mice

Next, we investigated whether treatment with a positive modulator of AMPARs could rescue the impairments observed in $Tm4sf2^{-/y}$ mice. To accomplish this, we evaluated synaptic function after either acute or chronic systemic treatment with the CX516. This compound acts as a positive allosteric modulator of AMPARs and was previously demonstrated to ameliorate deficits in AMPAR function and to improve behavioral performance (Hampson et al. 1998a, 1998b; Kanju et al. 2008; Broberg et al. 2009; Simmons et al. 2009).

Acute CX516 application (30 μM) fully restored AMPA-mEPSCs, normalized the excitation–inhibition balance and LTP in $Tm4sf2^{-/y}$ hippocampal slices (Supplementary Fig. 5A–C).

Similarly, chronic treatment with CX516 (5 mg/kg of CX516 or vehicle for 5 days) (Rex et al. 2006; Baudry et al. 2012) (Fig. 5A) induced an increase of surface expression of GluA2/3 ($Tm4sf2^{+/y}$+vehicle $n_{mice} = 4$: 1 ± 0 vs. $Tm4sf2^{-/y}$+vehicle $n_{mice} = 3$: 0.66 ± 0.08 vs. $Tm4sf2^{+/y}$+CX516 $n_{mice} = 3$: 1.26 ± 0.09 vs. $Tm4sf2^{-/y}$+CX516 $n_{mice} = 3$: 1.36 ± 0.24, *$P < 0.05$, one-way ANOVA followed by Newman–Keuls post test) (Supplementary Fig. 6 A) and completely restored the ratio between GluA1- and GluA2-containing AMPAR as showed by measuring AMPAR RI ($Tm4sf2^{+/y}$+vehicle $n_{cells} = 9$: 3.2 ± 0.3 vs. $Tm4sf2^{-/y}$+vehicle $n_{cells} = 8$: 5.5 ± 0.8 vs. $Tm4sf2^{+/y}$+CX516 $n_{cells} = 5$: 2.9 ± 0.2 vs. $Tm4sf2^{-/y}$+CX516 $n_{cells} = 7$: 3.20 ± 0.18, *$P < 0.05$, **$P < 0.01$, one-way ANOVA followed by Newman–Keuls post test) (Fig. 5B) as well as LTP ($Tm4sf2^{+/y}$+vehicle $n_{slices} = 6$: 176.0 ± 14.2% vs. $Tm4sf2^{-/y}$+vehicle $n_{slices} = 7$: 123.0 ± 7.6% vs. $Tm4sf2^{+/y}$+CX516 $n_{slices} = 5$: 205.1 ± 19.7% vs. $Tm4sf2^{-/y}$+CX516 $n_{slices} = 7$: 172.6 ± 6.8%, *$P < 0.05$, **$P < 0.01$, one-way ANOVA followed by Newman–Keuls post test) in $Tm4sf2^{-/y}$ mice (Fig. 5C). As expected, CX516 treatment slightly increased synaptic potentiation upon LTP in $Tm4sf2^{+/y}$ mice (Fig. 5C). Moreover, chronic CX516 administration restored the normal PSD length but had no effect on PSD thickness (Fig. 5D, E and Supplementary Table 3A). Thus, no significant recovery of PSD volume was observed (Fig. 5F). By contrast, drug administration induced full recovery of excitatory synapse density in $Tm4sf2^{-/y}$ mice (Fig. 5G and Supplementary Table 3A).

## CX516 Rescues ID-Like Behavior in $Tm4sf2^{-/y}$ Mice

After assessing the positive effects of chronic CX516 treatment on synaptic alterations in $Tm4sf2^{-/y}$ mice, we next examined whether this treatment could improve learning and memory defects in these mice.

The results showed that CX516 treatment did not modify motor function in either genotype based on the mean number of
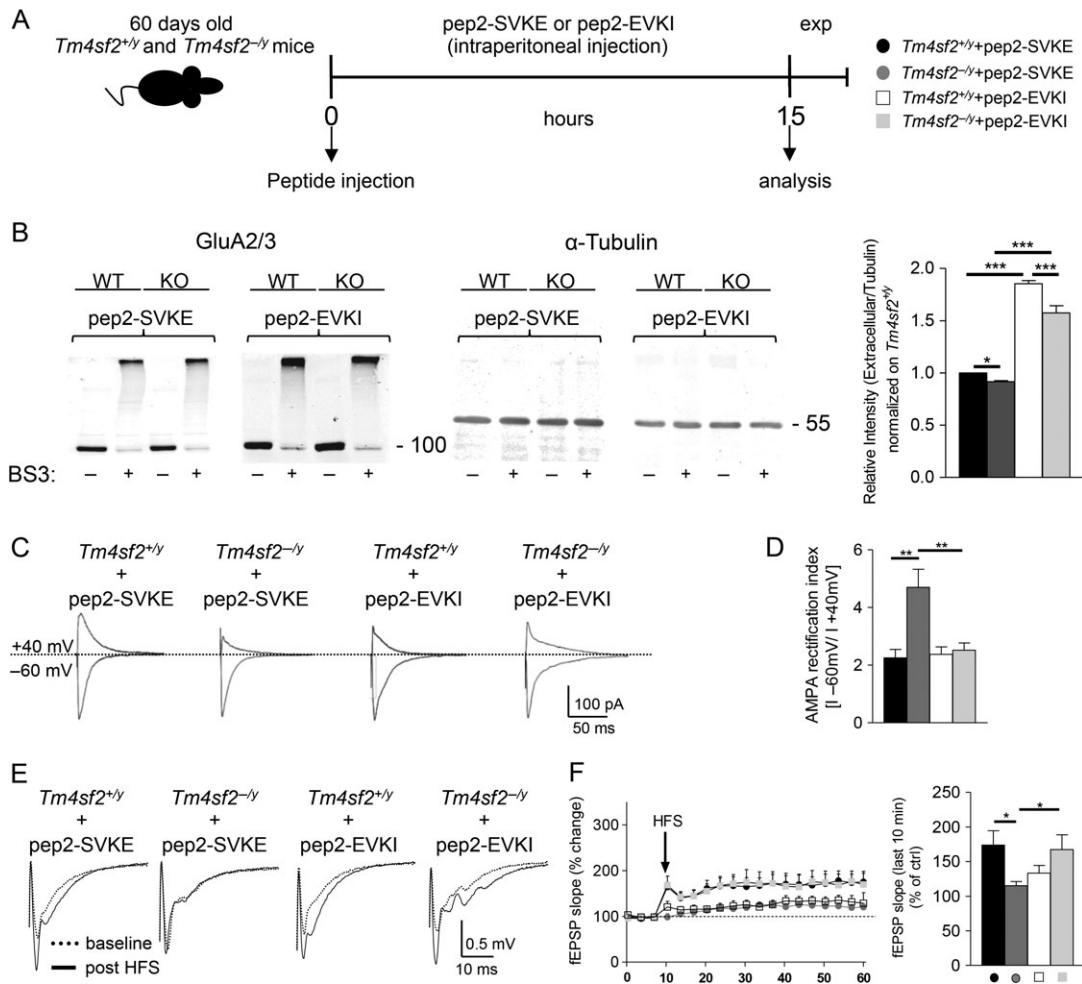
**Figure 4.** PICK1–GluA2 interference rescued RI and LTP in $Tm4sf2^{-/y}$ mice. (A) Representation of the peptide treatments. (B) Western blots and quantification of BS3 crosslinking assay in $Tm4sf2^{+/y}$ and $Tm4sf2^{-/y}$ mice treated for 15 h with the pep2-SVKE (inactive) or pep2-EVKI (active) peptides. Treatment with the active peptide (pep2-EVKI) increased GluA2/3 AMPAR subunit surface expression in the $Tm4sf2^{-/y}$ mice. (C,D) Representative traces of AMPA currents recorded at −60 and +40 mV from CA1 pyramidal neurons and quantification of AMPAR rectification index (RI) from $Tm4sf2^{+/y}$ and $Tm4sf2^{-/y}$ mice treated for 15 hrs with the pep2-SVKE (inactive) or pep2-EVKI (active) peptides. Treatment with the active peptide (pep2-EVKI), but not with the inactive peptide (pep2-EVKE), reverted the increased RI in the $Tm4sf2^{-/y}$ mice. (E,F) Representative traces of fEPSP recordings from the CA1 *stratum radiatum* before and after LTP induction from $Tm4sf2^{+/y}$ and $Tm4sf2^{-/y}$ mice treated 15 h before recordings with the pep2-SVKE (inactive) or pep2-EVKI (active) peptides. Treatment with the active peptide (pep2-EVKI), but not with the inactive peptide (pep2-EVKE), recovered LTP in the $Tm4sf2^{-/y}$ mice. (F) All data are represented as the mean ± S.E.M. Statistical comparison are stated in the main text.

horizontal and vertical counts taken over 30 min (Supplementary Fig. 7A, B). Notably, chronic treatment of CX516 improved episodic memory defects of $Tm4sf2^{-/y}$ mice in terms of increased discrimination index (Fig. 5H and Supplementary Table 3B) and mean exploration time to the novel object (Supplementary Fig. 8A). Furthermore, CX516 treatment rescued defects in spatial memory in $Tm4sf2^{-/y}$ mice, as assessed by the spatial object recognition task for discrimination index (Fig. 5I and Supplementary Table 3B) and mean exploration time to the displaced object (Supplementary Fig. 8B).

Chronic CX516 treatment also recovered associative memory in $Tm4sf2^{-/y}$ mice based on the results of auditory trace fear conditioning (ANOVA treatment effect $Tm4sf2^{-/y}$: $F_{1,43} = 5233$, *$P < 0.05$; ANOVA treatment effect $Tm4sf2^{+/y}$ : $F_{1,44} = 6,85$, $P < 0.05$) (Fig. 5L). Importantly, no significant difference was observed between $Tm4sf2^{-/y}$ mice treated with CX516 and $Tm4sf2^{+/y}$ mice, supporting the efficacy of the treatment. Collectively, these data clearly demonstrate that CX516 ameliorates learning and memory defects in $Tm4sf2^{-/y}$ mice, suggesting that positive AMPAR modulation is a potential new therapy for ID.

## Discussion

In the current study, we focused on evaluating the role of TSPAN7 in synapse function in vivo. To accomplish this, we characterized the functional, behavioral, and molecular phenotypes of $Tm4sf2^{-/y}$ mice. We found that neurons in $Tm4sf2^{-/y}$ mice have reductions in PSD length, thickness and volume as well as decreased excitatory synapse density. We also found that the absence of TSPAN7 causes reductions in the levels of GluA2- and GluA2/3-containing AMPARs at synapses but does not affect the presence of GluA1 or NMDAR subunit GluN1. Furthermore, $Tm4sf2^{-/y}$ mice showed increased AMPAR RI compared with $Tm4sf2^{+/y}$ mice indicating that the former had a decreased number of GluA2-containing AMPARs at the cell surface (Jackson and Nicoll 2011). As a result of this reduction and the observed decrease in spine density, the amplitude and frequency of AMPA-mEPSCs were decreased in $Tm4sf2^{-/y}$ mice (Aoto et al. 2015; Lee et al. 2015). We hypothesize that the thinning and decreased number of PSDs in the $Tm4sf2^{-/y}$ mice
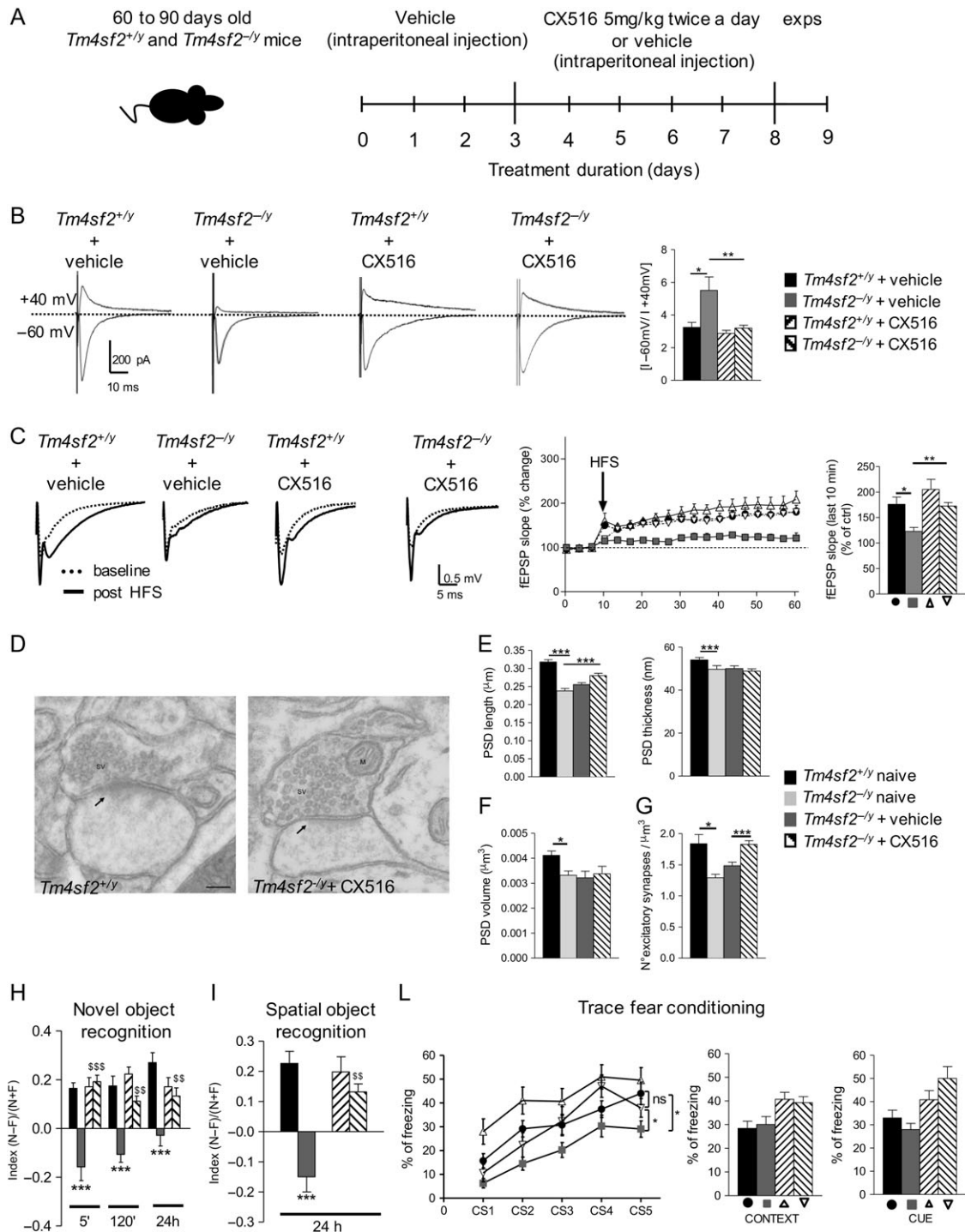
**Figure 5.** Chronic treatment with CX516 ameliorates synaptic and behavioral phenotypes in *Tm4sf2*$^{-/y}$ mice. (A) Representation of the treatment protocol. (B) Representative traces of AMPA currents recorded at −60 mV and +40 mV from CA1 pyramidal neurons and quantification of AMPAR rectification index (RI) from *Tm4sf2*$^{+/y}$ and *Tm4sf2*$^{-/y}$ mice chronically treated with vehicle or CX516. Treatment with CX516 reverted the increase in RI in the *Tm4sf2*$^{-/y}$ mice. (C) Representative traces of fEPSP recordings from the CA1 *stratum radiatum* before and after LTP induction from *Tm4sf2*$^{+/y}$ and *Tm4sf2*$^{-/y}$ mice chronically treated with vehicle or CX516. Treatment with CX516 recovered LTP in the *Tm4sf2*$^{-/y}$ mice. (D) Electron micrographs of asymmetrical synapses of the *stratum radiatum* of the hippocampal CA1 regions of *Tm4sf2*$^{+/y}$, *Tm4sf2*$^{-/y}$, *Tm4sf2*$^{-/y}$ +vehicle and *Tm4sf2*$^{-/y}$ +CX516 adult mice. Arrows indicate PSD. (E) On the right is the quantification of PSD length and thickness. (F) PSD volume. (G) Quantification of excitatory synapse density. (H) CX516 treatment rescued episodic memory as assessed using the novel object recognition task. (I) CX516 treatment rescued spatial memory as assessed using the spatial object recognition task. (L) Chronic treatment with CX516 improved the performance of *Tm4sf2*$^{-/y}$ mice in the trace fear conditioning test by ameliorating associative memory impairment. All data are represented as the mean ± S.E.M. Statistical comparison are stated in the main text and in Supplementary Table 3.

resulted from decreased synaptic activity due to reduced levels of GluA2- and GluA2/3-containing AMPARs. This is in agreement with previous reports indicating that PSDs are modified by synaptic activity (Dosemeci et al. 2001) and that increased expression of GluA3-containing AMPARs is linked to thicker PSDs (Clarkson et al. 2016).

Alterations in AMPARs have been reported in several animal models of ID (Calfa et al. 2015; Mignogna et al. 2015; Li et al. 2016) as well as in postmortem brains from patients with autism spectrum disorder (ASD) (Purcell et al. 2001). Additionally, AMPAR dysfunctions have been reported to alter the excitation/inhibition balance (Lee et al. 2017). In agreement with this relationship, we showed that CA1 pyramidal neurons in $Tm4sf2^{-/y}$ mice are less excitable than those in $Tm4sf2^{+/y}$ mice, suggesting an excitation/inhibition imbalance, which is a very common phenotype in neurological disorders (Nelson and Valakh 2015; Lee et al. 2017; Uzunova et al. 2016; Zapata et al. 2017).

Interestingly, LTP it is well known to depend on AMPARs and NMDARs activity (Neves et al., 2008). NMDA receptors at resting membrane potentials are blocked by $Mg^{2+}$, which is removed by AMPARs-mediated depolarization. For these reasons, we hypothesize that LTP impairment observed in $Tm4sf2^{-/y}$ mice could be due to the reduction of AMPARs whose activation will result insufficient to remove NMDARs $Mg^{2+}$ block thereby preventing $Ca^{2+}$ influx from triggering synapse potentiation (Lu et al. 2001; Lee et al. 2003; Oren et al. 2009). Indeed, when we bypassed AMPARs activation inducing LTP in $Mg^{2+}$-free condition we observed a complete recovery of LTP in $Tm4sf2^{-/y}$ mice, suggesting that our hypothesis was correct.

In accordance with their impaired LTP, $Tm4sf2^{-/y}$ mice showed defects in cognitive functions related to novel object recognition, spatial object recognition, water maze and fear conditioning tests. Moreover, fear conditioning task revealed that $Tm4sf2^{-/y}$ mice were impaired in the trace-conditioning paradigm, suggesting they also had reductions in associative cue learning. This finding is in agreement with the severe impairments in spatial and non-spatial memory that have been observed in GluA2-knockout mice (Gerlai et al. 1998). Furthermore, the disruptive effects on memory were due to nonspecific motor impairment because $Tm4sf2^{-/y}$ mice showed no impairment in locomotor activity. Notably, the $Tm4sf2^{-/y}$ mice showed defects in both phases of the water maze test as well as in trace fear conditioning, suggesting that other brain areas could be affected in these animals in addition to the hippocampus (Darvas and Palmiter 2011; Moustafa et al. 2013).

Notably, LTP and memory defects observed here are similar to the features of several neurodevelopmental disorders such as Angelman syndrome, Fragile X mental retardation (FMR) (Lauterborn et al. 2007; Lee et al. 2011), ASD (Bozdagi et al. 2010; Schmeisser et al. 2012; Won et al. 2012) and Rett syndrome (Belichenko et al. 2009).

Mechanistically, we previously reported that TSPAN7 competes with PICK1 for the binding with GluA2, regulating AMPAR trafficking in cultured neurons. TSPAN7 knockdown increases PICK1–GluA2/3 binding, which in turn augments the intracellular retention or internalization of GluA2-containing AMPARs (Bassani et al. 2012). Therefore, it is reasonable to believe that this mechanism occurs also in vivo. It is widely reported that AMPAR rectification increases when GluA2-containing AMPARs decrease (Washburn et al. 1997; Jackson and Nicoll 2011). In line with these observations, we demonstrated an increased AMPAR RI in $Tm4sf2^{-/y}$ mice reflecting a reduction in GluA2-containing AMPARs expression.

Following our hypothesis of an increased GluA2 AMPAR subunit internalization, we mimicked the function of TSPAN7 in $Tm4sf2^{-/y}$ mice using a synthetic peptide (pep2-EVKI) that has previously been shown to compete with the PICK1–GluA2 interaction. This approach was able to increase GluA2 AMPAR subunit surface expression in both $Tm4sf2^{+/y}$ and $Tm4sf2^{-/y}$ mice and to restore AMPAR RI and a normal LTP in $Tm4sf2^{-/y}$ mice, thus confirming in vivo the previously demonstrated TSPAN7 involvement in AMPAR trafficking.

We also found that boosting synaptic activity through treatment with the ampakine CX516 partially rescued synaptic structure, function and plasticity and ameliorated learning and memory defects in $Tm4sf2^{-/y}$ mice. Several studies reported that, in general, ampakines are molecules that readily cross the blood–brain barrier (Staubli et al. 1994; Ren et al. 2015) but no studies reported specifically the blood–brain barrier penetrance for CX516. However, CX516 was injected intraperitoneally in animals with positive effects on memory correlated to neuronal activity (Hampson et al. 1998a, 1998b) suggesting that also this molecule cross the blood–brain barrier. Furthermore, ampakines have previously been proposed as a pharmacological tool for the treatment of several neurological pathologies (Ogier et al. 2007; Simmons et al. 2011; Silverman et al. 2013); however, they have not been used to treat ID despite being shown to rescue AMPAR defects, enhance LTP, improve animal learning task performance and augment cognition in humans (Hampson et al. 1998a, 1998b; Lynch and Gall 2006; Wezenberg et al. 2007; Chang et al. 2014). Therefore, it is not surprising that CX516 rescued the aberrant phenotype in $Tm4sf2^{-/y}$ mice. Functionally, in $Tm4sf2^{-/y}$ mice, the administration of CX516 enhances AMPAR activity that could trigger the insertion of additional GluA2-containing AMPARs into the plasma membrane or drive extrasynaptic GluA2-containing AMPARs to the synapse, thereby recovering LTP, learning and memory.

In conclusion, our results indicate that positive allosteric modulation of AMPAR rescues the ID-like phenotype in $Tm4sf2^{-/y}$ mice and suggest that AMPAR could be a potential therapeutic target for ID.

## Supplementary Material

Supplementary data are available at *Cerebral Cortex* online.

## Notes

We thank M. Mameli and P. Botta for feedback on the manuscript and discussions. *Competing Interests Statement.* The authors declare that they have no competing financial interests.

## References

Abidi FE, Holinski-Feder E, Rittinger O, Kooy F, Lubs HA, Stevenson RE, Schwartz CE. 2002. A novel 2 bp deletion in the TM4SF2 gene is associated with MRX58. J Med Genet. 39: 430–433.

Adesnik H, Nicoll RA. 2007. Conservation of glutamate receptor 2-containing AMPA receptors during long-term potentiation. Neuroscientist. 27:4598–4602.

Andreu Z, Yanez-Mo M. 2014. Tetraspanins in extracellular vesicle formation and function. Front Immunol. 5:442.

Aoto J, Foldy C, Ilcus SM, Tabuchi K, Sudhof TC. 2015. Distinct circuit-dependent functions of presynaptic neurexin-3 at GABAergic and glutamatergic synapses. Nat Neurosci. 18: 997–1007.

Bassani S, Cingolani LA. 2012. Tetraspanins: interactions and interplay with integrins. Int J Biochem Cell Biol. 44:703–708.

Bassani S, Cingolani LA, Valnegri P, Folci A, Zapata J, Gianfelice A, Sala C, Goda Y, Passafaro M. 2012. The X-linked intellectual disability protein TSPAN7 regulates excitatory synapse development and AMPAR trafficking. Neuron. 73:1143–1158.

Bassani S, Passafaro M. 2012. TSPAN7: a new player in excitatory synapse maturation and function. Bioarchitecture. 2: 95–97.

Bassani S, Zapata J, Gerosa L, Moretto E, Murru L, Passafaro M. 2013. The neurobiology of X-linked intellectual disability. Neuroscientist. 19:541–552.

Baudry M, Kramar E, Xu X, Zadran H, Moreno S, Lynch G, Gall C, Bi X. 2012. Ampakines promote spine actin polymerization, long-term potentiation, and learning in a mouse model of Angelman syndrome. Neurobiol Dis. 47:210–215.

Belichenko PV, Wright EE, Belichenko NP, Masliah E, Li HH, Mobley WC, Francke U. 2009. Widespread changes in dendritic and axonal morphology in Mecp2-mutant mouse models of Rett syndrome: evidence for disruption of neuronal networks. J Comp Neurol. 514:240–258.

Bellone C, Luscher C. 2006. Cocaine triggered AMPA receptor redistribution is reversed in vivo by mGluR-dependent long-term depression. Nat Neurosci. 9:636–641.

Boucheix C, Rubinstein E. 2001. Tetraspanins. Cell Mol Life Sci. 58:1189–1205.

Bozdagi O, Sakurai T, Papapetrou D, Wang X, Dickstein DL, Takahashi N, Kajiwara Y, Yang M, Katz AM, Scattoni ML, et al. 2010. Haploinsufficiency of the autism-associated Shank3 gene leads to deficits in synaptic function, social interaction, and social communication. Mol Autism. 1:15.

Broberg BV, Glenthoj BY, Dias R, Larsen DB, Olsen CK. 2009. Reversal of cognitive deficits by an ampakine (CX516) and sertindole in two animal models of schizophrenia—subchronic and early postnatal PCP treatment in attentional set-shifting. Psychopharmacology (Berl). 206:631–640.

Burette A, Collman F, Micheva KD, Smith SJ, Weinberg RJ. 2015. Knowing a synapse when you see one. Front Neuroanat. 9:100.

Calfa G, Li W, Rutherford JM, Pozzo-Miller L. 2015. Excitation/inhibition imbalance and impaired synaptic inhibition in hippocampal area CA3 of Mecp2 knockout mice. Hippocampus. 25:159–168.

Chang PK, Prenosil GA, Verbich D, Gill R, McKinney RA. 2014. Prolonged ampakine exposure prunes dendritic spines and increases presynaptic release probability for enhanced long-term potentiation in the hippocampus. Eur J Neurosci. 40: 2766–2776.

Charrin S, Jouannet S, Boucheix C, Rubinstein E. 2014. Tetraspanins at a glance. J Cell Sci. 127:3641–3648.

Charrin S, le Naour F, Silvie O, Milhiet PE, Boucheix C, Rubinstein E. 2009. Lateral organization of membrane proteins: tetraspanins spin their web. Biochem J. 420:133–154.

Chavis P, Westbrook G. 2001. Integrins mediate functional pre- and postsynaptic maturation at a hippocampal synapse. Nature. 411:317–321.

Clarkson C, Antunes FM, Rubio ME. 2016. Conductive hearing loss has long-lasting structural and molecular effects on presynaptic and postsynaptic structures of auditory nerve synapses in the cochlear nucleus. Neuroscientist. 36: 10214–10227.

Darvas M, Palmiter RD. 2011. Contributions of striatal dopamine signaling to the modulation of cognitive flexibility. Biol Psychiatry. 69:704–707.

Denk W, Horstmann H. 2004. Serial block-face scanning electron microscopy to reconstruct three-dimensional tissue nanostructure. PLoS Biol. 2:e329.

Derkach VA, Oh MC, Guire ES, Soderling TR. 2007. Regulatory mechanisms of AMPA receptors in synaptic plasticity. Nat Rev Neurosci. 8:101–113.

Dosemeci A, Tao-Cheng JH, Vinade L, Winters CA, Pozzo-Miller L, Reese TS. 2001. Glutamate-induced transient modification of the postsynaptic density. Proc Natl Acad Sci U S A. 98: 10428–10432.

Folci A, Murru L, Vezzoli E, Ponzoni L, Gerosa L, Moretto E, Longo F, Zapata J, Braida D, Pistillo F, et al. 2016. Myosin IXa binds AMPAR and regulates synaptic structure, LTP, and cognitive function. Front Mol Neurosci. 9:1.

Gerlai R, Henderson JT, Roder JC, Jia Z. 1998. Multiple behavioral anomalies in GluR2 mutant mice exhibiting enhanced LTP. Behav Brain Res. 95:37–45.

Grutzendler J, Kasthuri N, Gan WB. 2002. Long-term dendritic spine stability in the adult cortex. Nature. 420:812–816.

Hampson RE, Rogers G, Lynch G, Deadwyler SA. 1998a. Facilitative effects of the ampakine CX516 on short-term memory in rats: correlations with hippocampal neuronal activity. Neuroscientist. 18:2748–2763.

Hampson RE, Rogers G, Lynch G, Deadwyler SA. 1998b. Facilitative effects of the ampakine CX516 on short-term memory in rats: enhancement of delayed-nonmatch-to-sample performance. Neuroscientist. 18:2740–2747.

Hemler ME. 1998. Integrin associated proteins. Curr Opin Cell Biol. 10:578–585.

Hemler ME. 2005. Tetraspanin functions and associated microdomains. Nat Rev Mol Cell Biol. 6:801–811.

Hemler ME. 2008. Targeting of tetraspanin proteins—potential benefits and strategies. Nat Rev Drug Discov. 7:747–758.

Hemler ME. 2014. Tetraspanin proteins promote multiple cancer stages. Nat Rev Cancer. 14:49–60.

Huerta PT, Sun LD, Wilson MA, Tonegawa S. 2000. Formation of temporal memory requires NMDA receptors within CA1 pyramidal neurons. Neuron. 25:473–480.

Jackson AC, Nicoll RA. 2011. Stargazin (TARP gamma-2) is required for compartment-specific AMPA receptor trafficking and synaptic plasticity in cerebellar stellate cells. Neuroscientist. 31:3939–3952.

Jiang X, Zhang J, Huang Y. 2015. Tetraspanins in cell migration. Cell Adh Migr. 9:406–415.

Jones EL, Demaria MC, Wright MD. 2011. Tetraspanins in cellular immunity. Biochem Soc Trans. 39:506–511.

Kanju PM, Parameshwaran K, Sims C, Bahr BA, Shonesy BC, Suppiramaniam V. 2008. Ampakine CX516 ameliorates functional deficits in AMPA receptors in a hippocampal slice model of protein accumulation. Exp Neurol. 214:55–61.

Lauterborn JC, Rex CS, Kramar E, Chen LY, Pandyarajan V, Lynch G, Gall CM. 2007. Brain-derived neurotrophic factor rescues synaptic plasticity in a mouse model of fragile X syndrome. Neuroscientist. 27:10685–10694.

Lee CC, Huang CC, Hsu KS. 2015. The phospholipid-binding protein SESTD1 negatively regulates dendritic spine density by interfering with Rac1-Trio8 signaling pathway. Sci Report. 5:13250.

Lee E, Lee J, Kim E. 2017. Excitation/inhibition imbalance in animal models of autism spectrum disorders. Biol Psychiatry. 81:838–847.

Lee HK, Takamiya K, Han JS, Man H, Kim CH, Rumbaugh G, Yu S, Ding L, He C, Petralia RS, et al. 2003. Phosphorylation of the AMPA receptor GluR1 subunit is required for synaptic plasticity and retention of spatial memory. Cell. 112:631–643.

Lee HY, Ge WP, Huang W, He Y, Wang GX, Rowson-Baldwin A, Smith SJ, Jan YN, Jan LY. 2011. Bidirectional regulation of dendritic voltage-gated potassium channels by the fragile X mental retardation protein. Neuron. 72:630–642.

Lee SA, Suh Y, Lee S, Jeong J, Kim SJ, Kim SJ, Park SK. 2017. Functional expression of dopamine D2 receptor is regulated by tetraspanin 7-mediated postendocytic trafficking. FASEB J. 31:2301–2313.

Levy S. 2014. Function of the tetraspanin molecule CD81 in B and T cells. Immunol Res. 58:179–185.

Li W, Xu X, Pozzo-Miller L. 2016. Excitatory synapses are stronger in the hippocampus of Rett syndrome mice due to altered synaptic trafficking of AMPA-type glutamate receptors. Proc Natl Acad Sci U S A. 113:E1575–E1584.

Lu W, Man H, Ju W, Trimble WS, MacDonald JF, Wang YT. 2001. Activation of synaptic NMDA receptors induces membrane insertion of new AMPA receptors and LTP in cultured hippocampal neurons. Neuron. 29:243–254.

Lynch G, Gall CM. 2006. Ampakines and the threefold path to cognitive enhancement. Trends Neurosci. 29:554–562.

Maecker HT, Todd SC, Levy S. 1997. The tetraspanin superfamily: molecular facilitators. FASEB J. 11:428–442.

Mignogna ML, Giannandrea M, Gurgone A, Fanelli F, Raimondi F, Mapelli L, Bassani S, Fang H, Van Anken E, Alessio M, et al. 2015. The intellectual disability protein RAB39B selectively regulates GluA2 trafficking to determine synaptic AMPAR composition. Nat Commun. 6:6504.

Morris RG, Garrud P, Rawlins JN, O'Keefe J. 1982. Place navigation impaired in rats with hippocampal lesions. Nature. 297: 681–683.

Moustafa AA, Gilbertson MW, Orr SP, Herzallah MM, Servatius RJ, Myers CE. 2013. A model of amygdala-hippocampal-prefrontal interaction in fear conditioning and extinction in animals. Brain Cogn. 81:29–43.

Nelson SB, Valakh V. 2015. Excitatory/inhibitory balance and circuit homeostasis in autism spectrum disorders. Neuron. 87:684–698.

Neves G, Cooke SF, Bliss TV. 2008. Synaptic plasticity, memory and the hippocampus: a neural network approach to causality. Nat Rev Neurosci. 9:65–75.

Ogier M, Wang H, Hong E, Wang Q, Greenberg ME, Katz DM. 2007. Brain-derived neurotrophic factor expression and respiratory function improve after ampakine treatment in a mouse model of Rett syndrome. Neuroscientist. 27:10912–10917.

Oren I, Nissen W, Kullmann DM, Somogyi P, Lamsa KP. 2009. Role of ionotropic glutamate receptors in long-term potentiation in rat hippocampal CA1 oriens-lacunosum moleculare interneurons. Neuroscientist. 29:939–950.

Pan D, Sciascia A 2nd, Vorhees CV, Williams MT. 2008. Progression of multiple behavioral deficits with various ages of onset in a murine model of Hurler syndrome. Brain Res. 1188:241–253.

Penzes P, Buonanno A, Passafaro M, Sala C, Sweet RA. 2013. Developmental vulnerability of synapses and circuits associated with neuropsychiatric disorders. J Neurochem. 126: 165–182.

Perez JL, Khatri L, Chang C, Srivastava S, Osten P, Ziff EB. 2001. PICK1 targets activated protein kinase Calpha to AMPA

receptor clusters in spines of hippocampal neurons and reduces surface levels of the AMPA-type glutamate receptor subunit 2. Neuroscientist. 21:5417–5428.

Piton A, Gauthier J, Hamdan FF, Lafreniere RG, Yang Y, Henrion E, Laurent S, Noreau A, Thibodeau P, Karemera L, et al. 2011. Systematic resequencing of X-chromosome synaptic genes in autism spectrum disorder and schizophrenia. Mol Psychiatry. 16:867–880.

Pitsikas N, Rigamonti AE, Cella SG, Locatelli V, Sala M, Muller EE. 2001. Effects of molsidomine on scopolamine-induced amnesia and hypermotility in the rat. Eur J Pharmacol. 426: 193–200.

Pizzamiglio L, Focchi E, Murru L, Tamborini M, Passafaro M, Menna E, Matteoli M, Antonucci F. 2016. New role of ATM in controlling GABAergic tone during development. Cereb Cortex. 26:3879–3888.

Purcell AE, Jeon OH, Zimmerman AW, Blue ME, Pevsner J. 2001. Postmortem brain abnormalities of the glutamate neurotransmitter system in autism. Neurology. 57:1618–1628.

Ren J, Ding X, Greer JJ. 2015. Ampakines enhance weak endogenous respiratory drive and alleviate apnea in perinatal rats. Am J Respir Crit Care Med. 191:704–710.

Rex CS, Lauterborn JC, Lin CY, Kramar EA, Rogers GA, Gall CM, Lynch G. 2006. Restoration of long-term potentiation in middle-aged hippocampus after induction of brain-derived neurotrophic factor. J Neurophysiol. 96:677–685.

Romanska HM, Berditchevski F. 2011. Tetraspanins in human epithelial malignancies. J Pathol. 223:4–14.

Schmeisser MJ, Ey E, Wegener S, Bockmann J, Stempel AV, Kuebler A, Janssen AL, Udvardi PT, Shiban E, Spilker C, et al. 2012. Autistic-like behaviours and hyperactivity in mice lacking ProSAP1/Shank2. Nature. 486:256–260.

Shors TJ, Beylin AV, Wood GE, Gould E. 2000. The modulation of Pavlovian memory. Behav Brain Res. 110:39–52.

Silverman JL, Oliver CF, Karras MN, Gastrell PT, Crawley JN. 2013. AMPAKINE enhancement of social interaction in the BTBR mouse model of autism. Neuropharmacology. 64: 268–282.

Simmons DA, Mehta RA, Lauterborn JC, Gall CM, Lynch G. 2011. Brief ampakine treatments slow the progression of Huntington's disease phenotypes in R6/2 mice. Neurobiol Dis. 41:436–444.

Simmons DA, Rex CS, Palmer L, Pandyarajan V, Fedulov V, Gall CM, Lynch G. 2009. Up-regulating BDNF with an ampakine rescues synaptic plasticity and memory in Huntington's disease knockin mice. Proc Natl Acad Sci U S A. 106:4906–4911.

Squire LR, Wixted JT, Clark RE. 2007. Recognition memory and the medial temporal lobe: a new perspective. Nat Rev Neurosci. 8:872–883.

Staubli U, Perez Y, Xu FB, Rogers G, Ingvar M, Stone-Elander S, Lynch G. 1994. Centrally active modulators of glutamate receptors facilitate the induction of long-term potentiation in vivo. Proc Natl Acad Sci U S A. 91:11158–11162.

Tarrant JM, Robb L, van Spriel AB, Wright MD. 2003. Tetraspanins: molecular organisers of the leukocyte surface. Trends Immunol. 24:610–617.

Terashima A, Pelkey KA, Rah JC, Suh YH, Roche KW, Collingridge GL, McBain CJ, Isaac JT. 2008. An essential role for PICK1 in NMDA receptor-dependent bidirectional synaptic plasticity. Neuron. 57:872–882.

Uzunova G, Pallanti S, Hollander E. 2016. Excitatory/inhibitory imbalance in autism spectrum disorders: Implications for interventions and therapeutics. World J Biol Psychiatry. 17: 174–186.

van Spriel AB. 2011. Tetraspanins in the humoral immune response. Biochem Soc Trans. 39:512–517.

Washburn MS, Numberger M, Zhang S, Dingledine R. 1997. Differential dependence on GluR2 expression of three characteristic features of AMPA receptors. Neuroscientist. 17: 9393–9406.

Wezenberg E, Verkes RJ, Ruigt GS, Hulstijn W, Sabbe BG. 2007. Acute effects of the ampakine farampator on memory and information processing in healthy elderly volunteers. Neuropsychopharmacology. 32:1272–1283.

Won H, Lee HR, Gee HY, Mah W, Kim JI, Lee J, Ha S, Chung C, Jung ES, Cho YS, et al. 2012. Autistic-like social behaviour in Shank2-mutant mice improved by restoring NMDA receptor function. Nature. 486:261–265.

Yauch RL, Hemler ME. 2000. Specific interactions among transmembrane 4 superfamily (TM4SF) proteins and phosphoinositide 4-kinase. Biochem J. 351(3):629–637.

Zapata J, Moretto E, Hannan S, Murru L, Longatti A, Mazza D, Benedetti L, Fossati M, Heise C, Ponzoni L, et al. 2017. Epilepsy and intellectual disability linked protein Shrm4 interaction with GABABRs shapes inhibitory neurotransmission. Nat Commun. 8:14536.

Zemni R, Bienvenu T, Vinet MC, Sefiani A, Carrie A, Billuart P, McDonell N, Couvert P, Francis F, Chafey P, et al. 2000. A new gene involved in X-linked mental retardation identified by analysis of an X;2 balanced translocation. Nat Genet. 24:167–170.

Zoller M. 2009. Tetraspanins: push and pull in suppressing and promoting metastasis. Nat Rev Cancer. 9:40–55.